

A divergence free C^0 -RIPG stream function formulation of the incompressible Stokes system with variable viscosity

Nathan Sime^{1,*}, Paul Houston², Cian R. Wilson¹, and Peter E. van Keken¹

¹Earth and Planets Laboratory, Carnegie Institution for Science, Washington, D.C., U.S.A.

²School of Mathematical Sciences, University of Nottingham, Nottingham, U.K.

*Corresponding author: Nathan Sime, nsime@carnegiescience.edu

September 15, 2023

Abstract

Pointwise divergence free velocity field approximations of the Stokes system are gaining popularity due to their necessity in precise modelling of physical flow phenomena. Several methods have been designed to satisfy this requirement; however, these typically come at a greater cost when compared with standard conforming methods, for example, because of the complex implementation and development of specialized finite element bases. Motivated by the desire to mitigate these issues for 2D simulations, we present a C^0 -interior penalty Galerkin (IPG) discretization of the Stokes system in the stream function formulation. In order to preserve a spatially varying viscosity this approach does not yield the standard and well known biharmonic problem. We further employ the so-called robust interior penalty Galerkin (RIPG) method; stability and convergence analysis of the proposed scheme is undertaken. The former, which involves deriving a bound on the interior penalty parameter is particularly useful to address the $\mathcal{O}(h^{-4})$ growth in the condition number of the discretized operator. Numerical experiments confirming the optimal convergence of the proposed method are undertaken. Comparisons with thermally driven buoyancy mantle convection model benchmarks are presented.

1 Introduction

1.1 Motivation

Large areas of computational fluid dynamics rely on the accurate solution of the Stokes system which requires correct satisfaction of the mass conservation equation. We are particularly interested in geophysical flow calculations that model slow convection in the Earth's mantle to help understand the Earth's thermal and chemical evolution (Bercovici, 2015; Ricard, 2015; Schubert et al., 2001). Specific applications include: the modeling of the recycling and subsequent mixing of oceanic crust (Brandenburg et al., 2008; Christensen and Hofmann, 1994) potentially within preexisting heterogeneity (Gülcher et al., 2021), the thermal and chemical evolution of subduction zones (Gerya et al., 2021; Wada and King, 2015); and the formation of hotspots and large igneous provinces by mantle plumes.

Exact, or at least approximately local, mass conservation is particularly important for particle methods (Christensen and Hofmann, 1994; Tackley and King, 2003; van Keken et al., 1997). It has been shown, for example, that significant artefacts can occur when using the popular Taylor–Hood (TH) finite element method for the numerical approximation of the Stokes system with particles. The TH element pair for velocity–pressure does not satisfy mass conservation locally. Such artefacts include the formation of holes and concretions in the particle distribution or the artificial settling of particles in gravity driven flows. Recent geodynamical examples demonstrating this are for purely compositionally-driven flow (Samuel, 2018; Sime et al., 2021), thermochemical convection (Jones et al., 2021; Pusok et al., 2017; Wang et al., 2015), and when mathematical fields represented by particles are advected (Maljaars et al., 2019, 2021; Sime et al., 2021, 2022). We demonstrate these artifacts in Figure 1 and further refer to Jenny et al. (2001); McDermott and Pope (2008).

In this paper we will explore a new approach to guarantee exact mass conservation. Here, we specifically consider the incompressible Stokes system in 2D in a simply connected domain; this covers many of the typical geometries that are frequently used in geodynamical applications (Brandenburg et al., 2008; Hernlund and Tackley, 2008; Jones et al., 2021; Li and McNamara, 2022). The extension to simple compressible flow modeling for mantle convection (Bossman and van Keken, 2013; Jarvis and McKenzie, 1980; Tackley, 2008) is possible in the same fashion as in the transition made from Sime et al. (2021) to Sime et al. (2022).

1.2 Context

Several numerical schemes have been developed to exactly satisfy mass conservation of the velocity approximation, denoted here by \mathbf{u}_h , in a pointwise sense, by which we mean that $\nabla \cdot \mathbf{u}_h(\mathbf{x}) = 0$ for all \mathbf{x} in the computational domain (e.g., Brezzi et al., 1985; Cockburn et al., 2011; John et al., 2017; Raviart and Thomas, 1977; Rhebergen and Wells, 2018, 2020; Scott and Vogelius, 1985).

In our recent work, which demonstrated the need for exact mass conservation (Jones et al., 2021; Sime et al., 2021, 2022), we employed an embedded discontinuous Galerkin–hybrid discontinuous Galerkin (HDG) method which yields a solenoidal velocity approximation (as developed in Rhebergen and Wells (2020) and implemented in Maljaars et al. (2021)). However, even with the utilization of static condensation, which factorizes the element-local problems in favor of the global system defined on the facets, the system assembly and computation of the solution is expensive. Seeking a more computationally efficient numerical scheme in the 2D setting is the key motivation of this article.

The general approach which the above mentioned numerical schemes exploit to achieve exact pointwise satisfaction of mass conservation is by ensuring that the divergence of the velocity approximation lies in the space in which we seek the pressure approximation, denoted by Q^h , i.e., that $\nabla \cdot \mathbf{u}_h \in Q^h$. These schemes typically require the definition of specialized finite element (FE) basis functions which may be difficult to implement. Libraries such as `basix` (Scroggs et al., 2022) simplify and automate the creation of these FE bases; however, the variational formulation, assembly and computational solution of these systems may remain difficult. Also, as previously mentioned above, assembling HDG systems via static condensation requires careful management to preserve scalable and efficient local assembly into a global system.

A popular alternative is to consider the biharmonic formulation of the Stokes system which provides an exactly divergence free approximation of the velocity. In this setting, the velocity is cast as the curl of an unknown potential field, i.e., $\mathbf{u}_h = \nabla \times \phi_h$, where ϕ_h is the FE approximation of the stream function. Hence, the numerical approximation of the velocity vector is trivially solenoidal. The standard FE discretization of the fourth-order biharmonic problem requires a C^1 conforming basis for the approximation of ϕ_h (e.g., Argyris et al., 1968; Morley, 1968) or, for

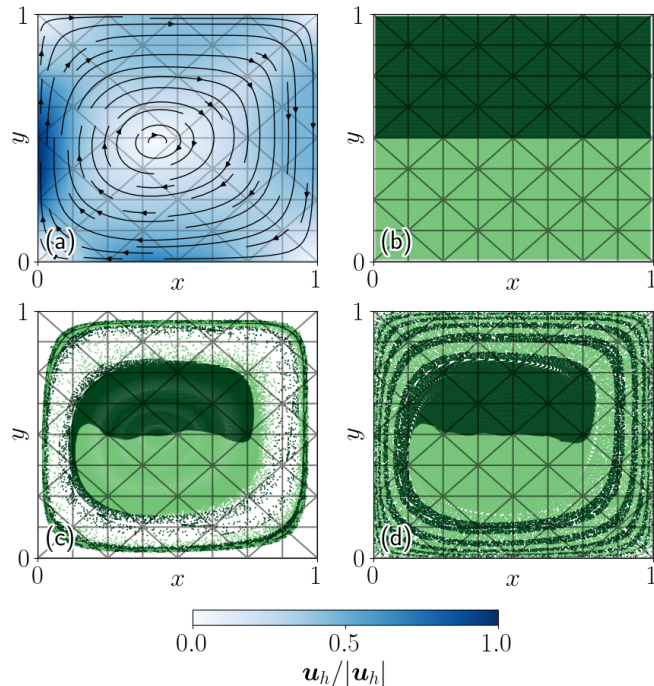


Figure 1: Advecting particles through velocity fields which are not pointwise divergence free may lead to spurious results. Here, we show an example advecting tracers using a third order accurate Runge–Kutta scheme in a mantle convection model exhibited as case T4 in our numerical experiments later in Section 5.2 (comprising a numerical benchmark in Tosi et al. (2015)). (a) The velocity field approximation computed using the C^0 -RIPG method developed in this work; shown are the computational mesh, velocity streamlines and normalized speed field. (b) The initial configuration of 256^2 equidistant particles colored solely as a visual aid. (c) The advected particles after approximately 10 overturns in a *non*-pointwise divergence free velocity field computed using the TH method. (d) The advected particles after approximately 10 overturns in the pointwise divergence free velocity field computed using the C^0 -RIPG method developed in this work. The average number of particles per cell is 512 with standard deviation of 36.67, 240.06 and 35.00 in (b), (c) and (d), respectively. The velocity field is discretized using polynomials of degree 2 in both the TH and C^0 -RIPG cases shown.

example, a C^k , $k \geq 1$, continuous divergence conforming B-spline basis (e.g., Christensen and Hofmann, 1994; Evans and Hughes, 2013; Kopitzke, 1979; van Keken et al., 1993).

In this work, our objective is to develop a FE formulation of the Stokes system by taking the same approach as the C^0 -interior penalty Galerkin (IPG) formulation of the biharmonic problem, whilst preserving the symmetric gradient operator permitting variable viscosity models. IPG methods in the context of discontinuous Galerkin (DG) FE discretizations for second order partial differential equations (PDEs) are well understood (see, for example, Arnold et al., 2001). In the context of fourth-order problems we seek to extend the technique presented in, for example, Engel et al. (2002); see also the recent complimentary paper by Dong and Mascotto (2023). In this setting, ϕ_h is approximated with a C^0 FE basis and continuity of its first derivative is enforced weakly. This formulation will yield many new terms on the facets of the FE mesh which may be verbose and arduous to implement. However, we exploit modern computational symbolic

specification (Alnæs et al., 2014) and automatic generation of FE formulations (Kirby and Logg, 2006) which vastly reduces implementation complexity.

Given this objective, we highlight what we see as clear advantages of the C^0 -IPG formulation and therefore our motivation:

1. Solenoidal velocity approximation.
2. Exploiting strong imposition of $\phi_h = 0$ on the computational boundary yields pointwise satisfaction of $\mathbf{u}_h \cdot \mathbf{n} = 0$, where \mathbf{n} denotes the unit outward pointing normal vector on the boundary of the computational domain.
3. In the context of the $2D$ system, reduction of the Stokes system's unknown velocity and pressure variables to a single unknown scalar potential.
4. Assembly using a standard C^0 FE basis with no special requirements.

However, we must highlight that the C^0 -IPG method does come with caveats:

1. The condition number of the underlying matrix stemming from the discretization of the fourth-order PDE exhibits growth at a rate of approximately h^{-4} as the mesh is uniformly refined; here, h is a measure of the mesh element size.
2. A dimensionless interior penalty parameter must be chosen to ensure stability of the scheme.
3. The matrix associated with the C^0 -IPG discretization is more dense than a standard conforming method.

Caveat 2 further impacts caveat 1 in the sense that the interior penalty parameter should be carefully selected not to be so large as to further adversely affect the condition number of the underlying matrix. For this reason, we employ the robust IPG (RIPG) formulation introduced in Dong and Georgoulis (2022). Here, the key modification to the underlying IPG scheme is the exploitation of a weighted average operator; this then allows for a lower bound on the interior penalty parameter to be determined in a simple manner.

1.3 Structure of the remainder of the paper

This article is structured as follows: in Section 2 we define the Stokes system and the associated stream function formulation. In Section 3 we define the C^0 -RIPG formulation, based on employing a suitable weighted average operator and interior penalty parameter. The stability and error analysis of the proposed scheme is studied in Section 4 where hp -optimal error bounds are established with respect to a given DG energy norm; this is in accordance with the analogous results derived in the case of a constant viscosity coefficient (Dong and Mascotto, 2023). The numerical performance of the C^0 -RIPG scheme is considered in Section 5. Finally, in Section 6 we summarize the work presented in this article and discuss potential future developments.

2 Stream function formulation

Let $\Omega \subset \mathbb{R}^2$ denote a simply connected domain with boundary $\partial\Omega$ and outward pointing unit normal vector \mathbf{n} . The boundary is subdivided into Dirichlet and Neumann components $\partial\Omega_D$ and

$\partial\Omega_N$, respectively, which do not overlap, i.e., $\partial\Omega_D \cup \partial\Omega_N = \partial\Omega$ and $\partial\Omega_D \cap \partial\Omega_N = \emptyset$. In Ω we seek the velocity $\mathbf{u} : \Omega \mapsto \mathbb{R}^2$ and pressure $P : \Omega \mapsto \mathbb{R}$ which satisfy the Stokes system

$$-\nabla \cdot (2\mu\varepsilon(\mathbf{u})) + \nabla P = \mathbf{f}, \quad (1)$$

$$\nabla \cdot \mathbf{u} = 0, \quad (2)$$

subject to the boundary conditions

$$\mathbf{u} = \mathbf{0} \quad \text{on } \partial\Omega_D, \quad (3)$$

$$2\mu\varepsilon(\mathbf{u}) \cdot \mathbf{n} - P\mathbf{n} = \mathbf{g}_N \quad \text{on } \partial\Omega_N. \quad (4)$$

Here, $\varepsilon(\mathbf{u}) = \frac{1}{2}(\nabla\mathbf{u} + \nabla\mathbf{u}^\top)$ is the symmetric gradient, $\mu(\mathbf{x}) : \Omega \mapsto \mathbb{R}^+$ is the viscosity, and $\mathbf{f}(\mathbf{x}) : \Omega \mapsto \mathbb{R}^2$ is a given forcing function.

Defining the space $\mathbf{H}_0^1(\Omega) = \{\mathbf{v} \in [H^1(\Omega)]^2 : \mathbf{v} = \mathbf{0} \text{ on } \partial\Omega_D\}$, the weak formulation of equations (1) and (2) reads: find $(\mathbf{u}, P) \in \mathbf{H}_0^1(\Omega) \times L_2(\Omega)$ such that

$$B(\mathbf{u}, \mathbf{v}) - (\nabla \cdot \mathbf{u}, P) = l(\mathbf{v}), \quad (5)$$

$$(\nabla \cdot \mathbf{u}, q) = 0 \quad (6)$$

for all $(\mathbf{v}, q) \in \mathbf{H}_0^1(\Omega) \times L_2(\Omega)$, where

$$B(\mathbf{u}, \mathbf{v}) = (2\mu\varepsilon(\mathbf{u}), \varepsilon(\mathbf{v})), \quad (7)$$

$$l(\mathbf{v}) = (\mathbf{f}, \mathbf{v}) + \langle \mathbf{g}_N, \mathbf{v} \rangle_{\partial\Omega_N}. \quad (8)$$

Here, (\cdot, \cdot) is the standard $L_2(\Omega)$ inner product and $\langle \cdot, \cdot \rangle_\omega$ denotes the $L_2(\omega)$ inner product on a subset ω of the boundary $\partial\Omega$.

Defining the divergence free space $\mathbf{Z}_0 = \{\mathbf{v} \in \mathbf{H}_0^1(\Omega) : \nabla \cdot \mathbf{v} = 0\}$ allows us to state the divergence free weak formulation: find $\mathbf{u} \in \mathbf{Z}_0$ such that

$$B(\mathbf{u}, \mathbf{v}) = l(\mathbf{v}) \quad \forall \mathbf{v} \in \mathbf{Z}_0. \quad (9)$$

Given that $\Omega \subset \mathbb{R}^2$ is simply connected, then for every $\mathbf{v} \in \mathbf{Z}_0$, there exists a unique $\psi \in H^2(\Omega) \setminus \mathbb{R}$ such that $\mathbf{v} = \nabla \times \psi$, where we define the curl vector acting on a scalar, $\psi : \Omega \mapsto \mathbb{R}$ and a vector, $\mathbf{z} = (\mathbf{z}_x, \mathbf{z}_y)^\top : \Omega \mapsto \mathbb{R}^2$, by

$$\nabla \times \psi = \left(\frac{\partial\psi}{\partial y}, -\frac{\partial\psi}{\partial x} \right)^\top \quad \text{and} \quad \nabla \times \mathbf{z} = \frac{\partial\mathbf{z}_y}{\partial x} - \frac{\partial\mathbf{z}_x}{\partial y}, \quad (10)$$

respectively, cf. Girault and Raviart (1986). Setting $\Psi_0 = \{\psi \in H^2(\Omega) \setminus \mathbb{R} : \nabla \times \psi = \mathbf{0} \text{ on } \partial\Omega_D\}$ we write the stream function formulation: find $\phi \in \Psi_0$ such that

$$B(\nabla \times \phi, \nabla \times \psi) = l(\nabla \times \psi) \quad \forall \psi \in \Psi_0. \quad (11)$$

3 C^0 -IPG formulation

Let \mathcal{T}^h be the subdivision of Ω into a mesh composed of a tessellation of nonoverlapping triangular elements κ such that $\mathcal{T}^h = \{\kappa\}$ and $\bar{\Omega} = \cup_{\kappa \in \mathcal{T}^h} \bar{\kappa}$. Each element has boundary $\partial\kappa$ with outward pointing unit normal vector \mathbf{n}_κ . The interior facets of the mesh are defined by $\Gamma_I = \cup_{\kappa \in \mathcal{T}^h} \partial\kappa \setminus \partial\Omega$, the exterior Dirichlet facets by $\Gamma_E = \cup_{\kappa \in \mathcal{T}^h} \partial\kappa \cap \partial\Omega_D$ and the mesh skeleton by $\Gamma = \Gamma_I \cup \Gamma_E$. Given

two neighboring elements κ^+ and κ^- and the smooth functions $\phi^\pm : \kappa^\pm \mapsto \mathbb{R}$ and $\mathbf{v}^\pm : \kappa^\pm \mapsto \mathbb{R}^2$, we define on their common face $F = \partial\kappa^+ \cap \partial\kappa^-$ the following operators

$$\{\!\!\{\phi\}\!\!\} = w^+ \phi^+ + w^- \phi^-, \quad (12)$$

$$\llbracket \mathbf{v} \rrbracket_\otimes = \mathbf{v}^+ \otimes \mathbf{n}^+ + \mathbf{v}^- \otimes \mathbf{n}^-, \quad (13)$$

which we refer to as the weighted average and tensor jump, respectively; for notational simplicity, here we write $\mathbf{n}^\pm = \mathbf{n}_{\kappa^\pm}$, respectively. On a boundary face $F = \partial\kappa \cap \partial\Omega_D$, we set $\{\!\!\{\phi\}\!\!\} = \phi$ and $\llbracket \mathbf{v} \rrbracket_\otimes = \mathbf{v} \otimes \mathbf{n}$, where \mathbf{n} denotes the outward unit normal vector on the boundary $\partial\Omega_D$. Here, the weights w^\pm are to be determined; however, they are subject to the constraint that $w^+ + w^- = 1$. Furthermore, we define the broken divergence, gradient, curl and symmetric gradient operators on each $\kappa \in \mathcal{T}^h$

$$(\nabla_h \cdot (\cdot))|_\kappa = \nabla \cdot (\cdot)|_\kappa, \quad (\nabla_h(\cdot))|_\kappa = \nabla(\cdot)|_\kappa, \quad (\nabla_h \times (\cdot))|_\kappa = \nabla \times (\cdot)|_\kappa, \quad \varepsilon_h(\cdot) = \frac{1}{2} \left(\nabla_h(\cdot) + \nabla_h(\cdot)^\top \right), \quad (14)$$

respectively.

We define the scalar FE function space

$$V_0^{h,p} = \{v \in H_0^1(\Omega) : v|_\kappa \in \mathcal{P}_p(\kappa) \ \forall \kappa \in \mathcal{T}^h\}, \quad (15)$$

where $H_0^1(\Omega) = \{v \in H^1(\Omega) : v = 0 \text{ on } \partial\Omega_D\}$, $\mathcal{P}_p(\kappa)$ denotes the polynomials of total degree p on κ , $\kappa \in \mathcal{T}^h$, and $p \geq 2$. Note that $V_0^{h,p} \not\subseteq \Psi_0$; hence, we will weakly impose the continuity of the derivatives of the underlying basis by employing the following C^0 -IPG scheme: find $\phi_h \in V_0^{h,p}$ such that

$$B_{\text{IP}}(\mathbf{u}_h, \mathbf{v}_h) = l_{\text{IP}}(\mathbf{v}_h) \quad \forall \psi_h \in V_0^{h,p}, \quad (16)$$

where $\mathbf{u}_h = \nabla_h \times \phi_h$, $\mathbf{v}_h = \nabla_h \times \psi_h$,

$$B_{\text{IP}}(\mathbf{u}, \mathbf{v}) = B_h(\mathbf{u}, \mathbf{v}) - \langle \llbracket \mathbf{u} \rrbracket_\otimes, \{\!\!\{2\mu\varepsilon_h(\mathbf{v})\}\!\!\} \rangle_\Gamma - \langle \{\!\!\{2\mu\varepsilon_h(\mathbf{u})\}\!\!\}, \llbracket \mathbf{v} \rrbracket_\otimes \rangle_\Gamma + \langle \beta \llbracket \mathbf{u} \rrbracket_\otimes, \llbracket \mathbf{v} \rrbracket_\otimes \rangle_\Gamma, \quad (17)$$

$B_h(\mathbf{u}, \mathbf{v}) = (2\mu\varepsilon_h(\mathbf{u}), \varepsilon_h(\mathbf{v}))$ and $l_{\text{IP}}(\cdot) = l(\cdot)$. Here, β is the interior penalty parameter which will be defined in the following section. A derivation of this C^0 -IPG formulation is outlined in Appendix A.

Remark 3.1. *In the case when inhomogeneous Dirichlet boundary conditions are employed, i.e., $\mathbf{u} = \mathbf{u}_D$ on $\partial\Omega_D$, we seek $\phi_h \in V^{h,p} = \{v \in H^1(\Omega) : v|_\kappa \in \mathcal{P}_p(\kappa) \ \forall \kappa \in \mathcal{T}^h\}$ such that*

$$B_{\text{IP}}(\mathbf{u}_h, \mathbf{v}_h) = l_{\text{IP}}(\mathbf{v}_h) \quad \forall \psi_h \in V^{h,p}, \quad (18)$$

where $l_{\text{IP}}(\cdot)$ is replaced by the alternative linear functional

$$l_{\text{IP}}(\mathbf{v}) = l(\mathbf{v}) + \langle \mathbf{u}_D \otimes \mathbf{n}, \beta \mathbf{v} \otimes \mathbf{n} - 2\mu\varepsilon_h(\mathbf{v}) \rangle_{\partial\Omega_D}. \quad (19)$$

Remark 3.2. *In the case of free slip and zero penetration conditions we divide $\partial\Omega_D$ into free slip and zero penetration components $\partial\Omega_{FS}$ and $\partial\Omega_{ZP}$, respectively, such that $\partial\Omega_D = \partial\Omega_{FS} \cup \partial\Omega_{ZP}$ and $\partial\Omega_{FS} \cap \partial\Omega_{ZP} = \emptyset$. On these components we impose*

$$\mathbf{u} \cdot \mathbf{n} = 0 \quad \text{on } \partial\Omega_{FS} \cup \partial\Omega_{ZP}, \quad (20)$$

$$(2\mu\varepsilon_h(\mathbf{u}) \cdot \mathbf{n} - P\mathbf{n}) \cdot \boldsymbol{\tau} = 0 \quad \text{on } \partial\Omega_{FS}. \quad (21)$$

$$\mathbf{u} \cdot \boldsymbol{\tau} = \mathbf{u}_D \cdot \boldsymbol{\tau} \quad \text{on } \partial\Omega_{ZP}, \quad (22)$$

where $\boldsymbol{\tau}$ is the unit vector which lies tangential to $\partial\Omega$. We may exploit the strong imposition of $\phi_h|_{\partial\Omega_D} = 0$ by seeking $\phi_h \in V_0^{h,p}$ such that

$$B_{IP}(\mathbf{u}_h, \mathbf{v}_h) = l_{IP}(\mathbf{v}_h) \quad \forall \psi_h \in V_0^{h,p}, \quad (23)$$

where $l_{IP}(\cdot)$ is the alternative linear functional

$$l_{IP}(\mathbf{v}) = l(\mathbf{v}) + \langle \mathbf{u}_D \otimes \mathbf{n}, \beta \mathbf{v} \otimes \mathbf{n} - 2\mu \varepsilon_h(\mathbf{v}) \rangle_{\partial\Omega_{ZF}}. \quad (24)$$

This scheme yields pointwise satisfaction of the boundary flux such that

$$\|\nabla_h \phi_h \cdot \boldsymbol{\tau}\|_{L_2(\partial\Omega_D)} = \|\nabla_h \times \phi_h \cdot \mathbf{n}\|_{L_2(\partial\Omega_D)} = \|\mathbf{u}_h \cdot \mathbf{n}\|_{L_2(\partial\Omega_D)} = 0. \quad (25)$$

3.1 C^0 -RIPG formulation

The classical symmetric interior penalty Galerkin (SIPG) formulation sets $w^\pm = \frac{1}{2}$. However we seek to exploit the RIPG formulation introduced in Dong and Georgoulis (2022) which is based on a particular choice of the weights w^\pm and the interior penalty parameter β . The key advantage of the RIPG formulation is that it remains parameterless in the sense that there is a known bound on β which ensures stability of the numerical scheme given appropriate choices of w^\pm . We first state the values we employ in the context of our 2D numerical experiments when \mathcal{T}^h is composed of triangles. In the remainder of this section we rationalize this choice based on studying the stability of the RIPG scheme, along with discussing the advantages when using this method when compared with a standard SIPG numerical scheme.

The RIPG scheme average operator weights and interior penalty parameter are defined, respectively, by

$$w^\pm = \frac{\zeta^\pm}{\zeta^+ + \zeta^-}, \quad \beta|_F = \begin{cases} (\zeta^+ + \zeta^-)^{-2} & F \subset \Gamma_I, \\ (\zeta^+)^{-2} & F \subset \Gamma_E, \end{cases} \quad (26)$$

where

$$\zeta^\pm|_F = \left(\delta \sqrt{\frac{3p(p-1)}{2} \frac{|F|}{|\kappa^\pm|}} \|2\mu \mathbf{n}^\pm\|_{L_\infty(F)} \|(2\mu)^{-\frac{1}{2}}\|_{L_\infty(\kappa^\pm)} \right)^{-1}, \quad (27)$$

where for a set $\omega \subset \mathbb{R}^n$, $n \geq 1$, we write $|\omega|$ to denote the n -dimensional Hausdorff measure of ω and $\delta > \sqrt{2}$ is a constant, cf. below.

4 Stability and error analysis

The aim of this section is to study the stability of the C^0 -RIPG formulation (16) and establish an optimal hp -error bound. For the purposes of the proceeding error analysis we introduce a suitable extension of the bilinear form $B_{IP}(\cdot, \cdot)$. To this end, we write $\Pi_{L_2} : [L_2(\Omega)]^{2 \times 2} \mapsto [V^{h,p-2}]^{2 \times 2}$ to denote the orthogonal L_2 -projection operator. With this notation for $\phi, \psi \in V := H^2(\Omega) + V_0^{h,p}$ we write

$$\tilde{B}_{IP}(\mathbf{u}, \mathbf{v}) = B_h(\mathbf{u}, \mathbf{v}) - \langle \llbracket \mathbf{u} \rrbracket_\otimes, \{ \{ 2\mu \Pi_{L_2}(\varepsilon_h(\mathbf{v})) \} \} \rangle_\Gamma - \langle \{ \{ 2\mu \Pi_{L_2}(\varepsilon_h(\mathbf{u})) \} \}, \llbracket \mathbf{v} \rrbracket_\otimes \rangle_\Gamma + \langle \beta \llbracket \mathbf{u} \rrbracket_\otimes, \llbracket \mathbf{v} \rrbracket_\otimes \rangle_\Gamma, \quad (28)$$

where $\mathbf{u} = \nabla_h \times \phi$ and $\mathbf{v} = \nabla_h \times \psi$. Furthermore, we introduce the following DG norm

$$\|\mathbf{v}\|_{IP}^2 = \left\| \sqrt{2\mu} \varepsilon_h(\mathbf{v}) \right\|_{L_2(\Omega)}^2 + \left\| \sqrt{\beta} \llbracket \mathbf{v} \rrbracket_\otimes \right\|_{L_2(\Gamma)}^2. \quad (29)$$

4.1 Coercivity and continuity

The aim of this section is to study the stability of the C^0 -RIPG scheme (16). To this end, we first recall the following inverse equality from Warburton and Hesthaven (2003).

Lemma 4.1. *Given $\kappa \in \mathcal{T}^h$ is a triangular element in 2D ($d = 2$ below), let $F \subset \partial\kappa$ denote one of its faces. Then for $v \in \mathcal{P}_p(\kappa)$ the following inverse inequality holds*

$$\|v\|_{L_2(F)} \leq C_{inv}(\kappa, F, p) \|v\|_{L_2(\kappa)}, \quad (30)$$

where

$$C_{inv}(\kappa, F, p) = \sqrt{\frac{(p+1)(p+d)}{d} \frac{|F|}{|\kappa|}}. \quad (31)$$

Equipped with Lemma 4.1 we now state the main result of this section.

Lemma 4.2. *The bilinear form $\tilde{B}_{IP}(\cdot, \cdot)$ is coercive for any $\delta > \sqrt{2}$ and continuous over $V \times V$; in particular we have that*

$$\begin{aligned} \tilde{B}_{IP}(\mathbf{v}, \mathbf{v}) &\geq C_{coer} \|\mathbf{v}\|_{IP}^2 && \forall \phi \in V, \\ \tilde{B}_{IP}(\mathbf{v}, \mathbf{w}) &\leq C_{cont} \|\mathbf{v}\|_{IP} \|\mathbf{w}\|_{IP} && \forall \phi, \psi \in V, \end{aligned}$$

where $\mathbf{v} = \nabla_h \times \phi$, $\mathbf{w} = \nabla_h \times \psi$, $C_{coer} = 1 - \sqrt{2}/\delta$ and $C_{cont} = 2(1 + 2/\delta^2)$.

Proof. We first consider the coercivity of the bilinear form $\tilde{B}_{IP}(\cdot, \cdot)$. For $\phi \in V$, $\mathbf{v} = \nabla_h \times \phi$, we note that

$$\tilde{B}_{IP}(\mathbf{v}, \mathbf{v}) = \left\| \sqrt{2\mu} \varepsilon_h(\mathbf{v}) \right\|_{L_2(\Omega)}^2 + \left\| \sqrt{\beta} [\mathbf{v}]_{\otimes} \right\|_{L_2(\Gamma)}^2 - 2 \int_{\Gamma} \{ \{ 2\mu \Pi_{L_2}(\varepsilon_h(\mathbf{v})) \} \} \cdot [\mathbf{v}]_{\otimes} \, ds. \quad (32)$$

In order to determine the lower bound on δ , we must express the last term in equation (32) in terms of the first two. Exploiting the inverse inequality stated in Lemma 4.1, together with the stability of the L_2 -projection operator Π_{L_2} , for interior faces, we deduce that

$$\begin{aligned} &\left| 2 \int_{\Gamma_I} \{ \{ 2\mu \Pi_{L_2}(\varepsilon_h(\mathbf{v})) \} \} \cdot [\mathbf{v}]_{\otimes} \, ds \right| \\ &\leq 2 \sum_{F \in \Gamma_I} \int_F \left(\sum_{* \in \{+, -\}} w^* \|2\mu \mathbf{n}^*\|_{L_{\infty}(F)} |\Pi_{L_2}(\varepsilon_h(\mathbf{v}^*))| \right) |[\mathbf{v}]_{\otimes}| \, ds \\ &\leq 2 \sum_{F \in \Gamma_I} \sum_{* \in \{+, -\}} \alpha^* w^* \left\| \sqrt{2\mu} \varepsilon_h(\mathbf{v}^*) \right\|_{L_2(\kappa^*)} \left\| [\mathbf{v}]_{\otimes} \right\|_{L_2(F)}, \end{aligned} \quad (33)$$

where

$$\alpha^* = C_{inv}(\kappa^*, F, p_{\kappa^*} - 2) \|2\mu \mathbf{n}^*\|_{L_{\infty}(F)} \left\| (2\mu)^{-\frac{1}{2}} \right\|_{L_{\infty}(\kappa^*)}. \quad (34)$$

In order to proceed, following (26) and (27), we select

$$w^* = \frac{\zeta^*}{\zeta^+ + \zeta^-}, \quad \zeta^* = \frac{1}{\delta \sqrt{m_{\kappa^*} \alpha^*}}, \quad (35)$$

respectively, where m_{κ^*} is the number of facets belonging to element κ^* , i.e., here $m_{\kappa^*} = 3$, and δ is a positive constant to be determined. Thereby, we deduce that

$$\begin{aligned} & \left| 2 \int_{\Gamma_I} \{2\mu \Pi_{L_2}(\varepsilon_h(\mathbf{v}))\} \cdot \llbracket \mathbf{v} \rrbracket_{\otimes} ds \right| \\ & \leq 2 \sum_{F \in \Gamma_I} \sum_{* \in \{+, -\}} \frac{1}{\delta \sqrt{m_{\kappa^*}}} \frac{1}{\zeta^+ + \zeta^-} \left\| \sqrt{2\mu} \varepsilon_h(\mathbf{v}^*) \right\|_{L_2(\kappa^*)} \left\| \llbracket \mathbf{v} \rrbracket_{\otimes} \right\|_{L_2(F)} \\ & \leq 2 \sum_{F \in \Gamma_I} \sum_{* \in \{+, -\}} \left(\frac{1}{2\epsilon} \frac{1}{\delta^2 m_{\kappa^*}} \left\| \sqrt{2\mu} \varepsilon_h(\mathbf{v}^*) \right\|_{L_2(\kappa^*)}^2 + \frac{\epsilon}{2} \beta \left\| \llbracket \mathbf{v} \rrbracket_{\otimes} \right\|_{L_2(F)}^2 \right), \end{aligned}$$

where $\epsilon > 0$ is a constant. An analogous bound can also be established for faces on the boundary of Ω . Hence, combining both bounds and observing the inequality

$$\sum_{F \in \Gamma} \sum_{* \in \{+, -\}} \|z^*\|_{L_2(\kappa^*)}^2 \leq \sum_{\kappa \in \mathcal{T}_h} m_{\kappa} \|z\|_{L_2(\kappa)}^2, \quad (36)$$

gives

$$\left| 2 \int_{\Gamma} \{2\mu \Pi_{L_2}(\varepsilon_h(\mathbf{v}))\} \cdot \llbracket \mathbf{v} \rrbracket_{\otimes} ds \right| \leq \frac{1}{\delta^2 \epsilon} \sum_{\kappa \in \mathcal{T}_h} \left\| \sqrt{2\mu} \varepsilon_h(\mathbf{v}) \right\|_{L_2(\kappa)}^2 + 2\epsilon \sum_{F \in \Gamma} \beta \left\| \llbracket \mathbf{v} \rrbracket_{\otimes} \right\|_{L_2(F)}^2, \quad (37)$$

from which we deduce that

$$\tilde{B}_{\text{IP}}(\mathbf{v}, \mathbf{v}) \geq \left(1 - \frac{1}{\delta^2 \epsilon}\right) \left\| \sqrt{2\mu} \varepsilon_h(\mathbf{v}) \right\|_{L_2(\Omega)}^2 + (1 - 2\epsilon) \left\| \sqrt{\beta} \llbracket \mathbf{v} \rrbracket_{\otimes} \right\|_{L_2(\Gamma)}^2. \quad (38)$$

To determine the unknown parameters δ and ϵ we set

$$\left(1 - \frac{1}{\delta^2 \epsilon}\right) = (1 - 2\epsilon) \implies \epsilon = \frac{1}{\sqrt{2}\delta}, \quad (39)$$

which, provided $\delta > \sqrt{2}$, yields a coercive numerical scheme.

The proof of continuity follows based on employing a similar argument and hence the details are omitted. \square

4.2 C^0 -RIPG convergence

In this section we now proceed to derive an hp -version a priori error bound for the C^0 -RIPG formulation (16). For simplicity of presentation, throughout this section we assume that \mathcal{T}^h is a quasi-uniform triangular mesh with (global) mesh element size parameter h . For the proceeding analysis we require an approximation result for the finite element space $V_0^{h,p}$. Given $v \in H^k(\Omega)$, $k \geq 3$, we assume there exists $\mathcal{G} : H^2(\Omega) \mapsto H^2(\Omega) \cap V_0^{h,p}$ such that

$$|v - \mathcal{G}v|_{H^s(\Omega)} \leq C \frac{h^{\mu-s}}{p^{k-s}} \|v\|_{H^k(\Omega)}, \quad (40)$$

where $\mu = \min(p+1, k)$ and C is a positive constant independent of h , p , v , and $\mathcal{G}v$. For triangular meshes in 2D this result was proved in Suri (1990) for $s = 0, 1, 2$; see Dong and Mascotto (2023) for analogous approximation results on tensor product meshes.

Equipped with (40) we now state the main result of this section.

Theorem 4.3. *Given that \mathcal{T}^h is a quasi-uniform triangular mesh, write $\mathbf{u} = \nabla \times \phi$ and $\mathbf{u}_h = \nabla_h \times \phi_h$ to denote the solutions to (11) and (16), respectively. Then assuming that $\phi \in H^k(\Omega)$, $k \geq 3$, we have that*

$$\|\mathbf{u} - \mathbf{u}_h\|_{\text{IP}} \leq C \frac{h^{\mu-2}}{p^{k-2}} \|\phi\|_{H^k(\Omega)},$$

where $\mu = \min(p+1, k)$ and C is a positive constant, which is independent of h and p .

Proof. For $\mathbf{u} = \nabla \times \phi$ and $\mathbf{u}_h = \nabla_h \times \phi_h$ we recall Strang's lemma

$$\begin{aligned} \|\mathbf{u} - \mathbf{u}_h\|_{\text{IP}} &\leq \left(1 + \frac{C_{\text{cont}}}{C_{\text{coer}}}\right) \inf_{\mathbf{v}_h = \nabla_h \times \psi_h, \psi_h \in V_0^{h,p}} \|\mathbf{u} - \mathbf{v}_h\|_{\text{IP}} \\ &\quad + \frac{1}{C_{\text{coer}}} \sup_{\mathbf{w}_h = \nabla_h \times \varphi_h, \varphi_h \in V_0^{h,p} \setminus \{0\}} \frac{|\tilde{B}_{\text{IP}}(\mathbf{u}, \mathbf{w}_h) - \ell(\mathbf{w}_h)|}{\|\mathbf{w}_h\|_{\text{IP}}}. \end{aligned} \quad (41)$$

Employing the approximation result (40), together with the H^2 -conformity of \mathcal{G} , the first term on the right-hand side of (41) can be bounded as follows

$$\begin{aligned} \inf_{\mathbf{v}_h = \nabla_h \times \psi_h, \psi_h \in V_0^{h,p}} \|\mathbf{u} - \mathbf{v}_h\|_{\text{IP}} &\leq \|\nabla \times \phi - \nabla_h \times (\mathcal{G}\phi)\|_{\text{IP}} \\ &= \left\| \sqrt{2\mu} \varepsilon_h (\nabla \times \phi - \nabla_h \times (\mathcal{G}\phi)) \right\|_{L_2(\Omega)} \leq C \frac{h^{\mu-2}}{p^{k-2}} \|\phi\|_{H^k(\Omega)}, \end{aligned}$$

as required.

For the second (consistency) term, noting that $\phi \in H^k(\Omega)$, $k \geq 3$, upon application of integration by parts and the Cauchy-Schwarz inequality, we deduce that

$$\begin{aligned} \tilde{B}_{\text{IP}}(\mathbf{u}, \mathbf{w}_h) - \ell(\mathbf{w}_h) &= \langle \{2\mu(\varepsilon_h(\mathbf{u}) - \Pi_{L_2} \varepsilon_h(\mathbf{u}))\}, \llbracket \mathbf{w}_h \rrbracket_{\otimes} \rangle_{\Gamma} \\ &\leq \|\beta^{-1/2} \{2\mu(\varepsilon_h(\mathbf{u}) - \Pi_{L_2} \varepsilon_h(\mathbf{u}))\}\|_{L_2(\Gamma)} \|\sqrt{\beta} \llbracket \mathbf{w}_h \rrbracket_{\otimes}\|_{L_2(\Gamma)}. \end{aligned}$$

We now recall the following approximation result from Chernov (2012) for the L_2 -projector. With a slight abuse of notation, we also write $\Pi_{L_2} : L_2(\kappa) \mapsto \mathcal{P}_p(\kappa)$ to denote the elementwise (scalar-valued) L_2 -projector. With this notation, given a triangular element $\kappa \in \mathcal{T}^h$, let $F \subset \partial\kappa$ denote one of its faces. Then, for $v \in H^k(\kappa)$, $k \geq 1$, the following bound holds

$$\|v - \Pi_{L_2} v\|_{L_2(F)} \leq C \frac{h^{\mu-1/2}}{p^{k-1/2}} \|v\|_{H^k(\kappa)}, \quad (42)$$

where $\mu = \min(p+1, k)$ and C is a positive constant independent of h , p , v , and $\Pi_{L_2} v$.

Equipped with (42), the definition of β , cf. (26) and the DG norm (29), we get

$$\tilde{B}_{\text{IP}}(\mathbf{u}, \mathbf{w}_h) - \ell(\mathbf{w}_h) \leq C \frac{h^{\mu-2}}{p^{k-3/2}} \|\phi\|_{H^k(\Omega)} \|\mathbf{w}_h\|_{\text{IP}}.$$

Collecting the above bounds gives the desired result. \square

Remark 4.4. *We remark that the bound derived in Theorem 4.3 is optimal in both the mesh element size h and the polynomial degree p ; this is in agreement to the analogous bound derived for the standard C^0 -IPG scheme in Dong and Mascotto (2023) for the Dirichlet problem. In the case when inhomogeneous Dirichlet boundary conditions are employed, then as in the case of second-order linear elliptic partial differential equations p -optimality is no longer possible, cf. Georgoulis et al. (2009).*

5 Numerical experiments

In this section we present a series of numerical experiments to investigate the practical performance of the proposed C^0 -RIPG scheme. We note that all of the computational examples have been implemented using the components of the FEniCS project (Logg et al., 2012). We highlight the Unified Form Language (UFL) (Alnæs et al., 2014) in particular as it facilitates the straightforward specification of the verbose facet terms arising in the C^0 -RIPG formulation (16). Initial prototypes of the C^0 -IPG and SIPG formulations were developed with the principles outlined in Houston and Sime (2018). The code used to generate the results presented here is available in Sime (2023).

Our experiments are constructed in two settings to test the numerical scheme. Firstly, we present a numerical example with a known analytical solution in order to validate the optimality of the a priori error bound derived in Theorem 4.3. Secondly, we study the performance of the proposed C^0 -RIPG scheme in the practical setting of reproducing benchmarks in mantle convection cell models. We examine the benefits of the C^0 -RIPG scheme's pointwise divergence free velocity approximation when coupled with advection of a scalar (temperature) field, in addition to its performance with viscosity models which are composed of variations over many orders of magnitude.

5.1 Manufactured solution

In this section, we let $\Omega = (-1, 1)^2$ be a square. We subdivide Ω into a hierarchy of meshes composed of $N \times N$ shape regular quadrilaterals each bisected into triangle elements, where $N \in \{8, 16, 32, 64, 128\}$ is the number of quadrilaterals dividing each orthogonal direction of Ω . We select the analytical solution and viscosity to be

$$\phi = \pi^{-1} \sin(\pi x) \sin(\pi y) \text{ and } \mu = 1 + \sin^2(\pi x) \sin^2(\pi y), \quad (43)$$

respectively, such that

$$\mathbf{u} = \begin{pmatrix} \sin(\pi x) \cos(\pi y) \\ -\cos(\pi x) \sin(\pi y) \end{pmatrix}, \quad (44)$$

which then determines \mathbf{f} according to equation (1). We compute approximations of ϕ using the C^0 -RIPG formulation and examine the rate at which the numerical approximation converges to the analytical solution. Furthermore, we examine the influence of the parameter δ on the stability of the numerical scheme. Here, the approximation error is measured in the DG-norm (29), as well as the following norms of interest:

$$\|\phi - \phi_h\|_{L_2(\mathcal{T}^h)}^2 = \sum_{\kappa \in \mathcal{T}^h} \int_{\kappa} (\phi - \phi_h)^2 d\mathbf{x}, \quad (45)$$

$$\|\mathbf{u} - \mathbf{u}_h\|_{L_2(\mathcal{T}^h)}^2 = \sum_{\kappa \in \mathcal{T}^h} \int_{\kappa} (\mathbf{u} - \nabla \times \phi_h)^2 d\mathbf{x}, \quad (46)$$

$$|\mathbf{u} - \mathbf{u}_h|_{H^1(\mathcal{T}^h)}^2 = \sum_{\kappa \in \mathcal{T}^h} \int_{\kappa} (\nabla \mathbf{u} - \nabla(\nabla \times \phi_h))^2 d\mathbf{x}. \quad (47)$$

In Figure 2 we plot the error measured in the above norms against the mesh element size h on the aforementioned sequence of uniform (structured) triangular meshes for $p = 2, 3, 4$. Here, we observe that for each fixed p , the DG norm of the error tends to zero at the optimal rate of $\mathcal{O}(h^{p-1})$ as h tends to zero; this is in full agreement with the predicted rate given in Theorem 4.3.

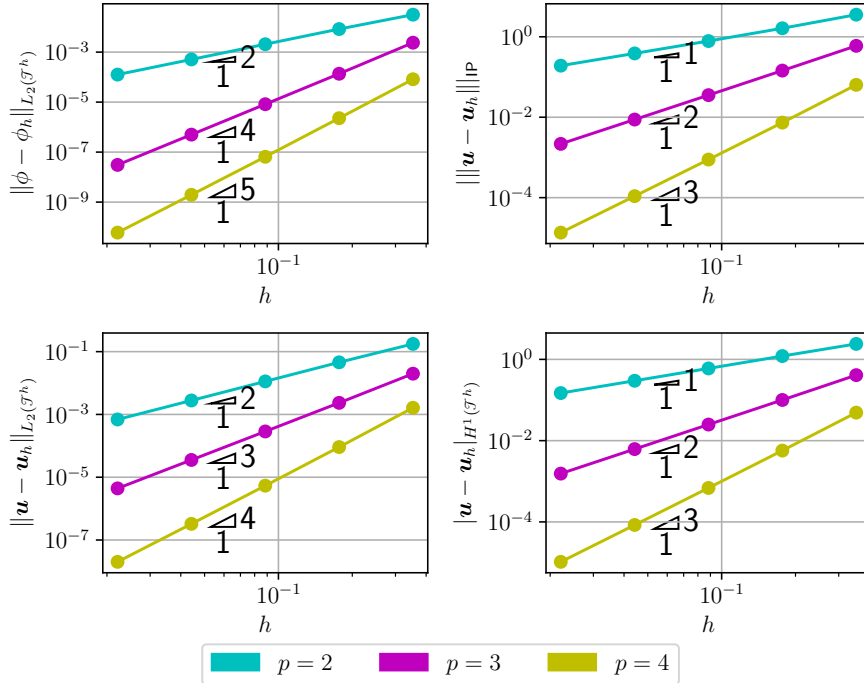


Figure 2: Measured error norms of the manufactured solution problem.

Analogous rates are observed for $|\mathbf{u} - \mathbf{u}_h|_{H^1(\mathcal{J}^h)}^2$ as expected. The $L_2(\Omega)$ norm of the error in the approximation to the velocity is observed to behave like $\mathcal{O}(h^p)$ as h tends to zero, which are again expected. However, we observe that $\|\phi - \phi_h\|_{L_2(\mathcal{J}^h)}^2 = \mathcal{O}(h^2)$ for $p = 2$, while $\|\phi - \phi_h\|_{L_2(\mathcal{J}^h)}^2 = \mathcal{O}(h^{p+1})$ for $p = 3, 4$, as h tends to zero, which indicates suboptimality in the approximation of the stream function when the error is measured in $L_2(\Omega)$ norm and the lowest order approximation is employed.

In Figure 3 we study the influence of the parameter δ on the stability of the C^0 -RIPG scheme and the approximation error. As indicated in Section 4.1 we observe that setting the penalty parameter $\delta > \sqrt{2}$ guarantees stability of the underlying method. We also see that smaller values of δ may be employed in practice which lead to a slight improvement of the error measured in the above norms. However, as expected if δ is reduced too far, then the stability of the C^0 -RIPG scheme is no longer guaranteed.

5.2 Buoyancy-driven flow

To examine the practicality of the C^0 -RIPG method we reproduce numerical benchmarks in the context of geophysical flow driven by thermal buoyancy. These benchmarks further employ temperature and strain-rate dependent viscosity models as exhibited in the works Blankenbach et al. (1989) and Tosi et al. (2015). These benchmarks require that $\Omega = (0, 1)^2$ is the unit square, in which we seek the velocity and pressure which satisfy equations (1) and (2) subject to the free

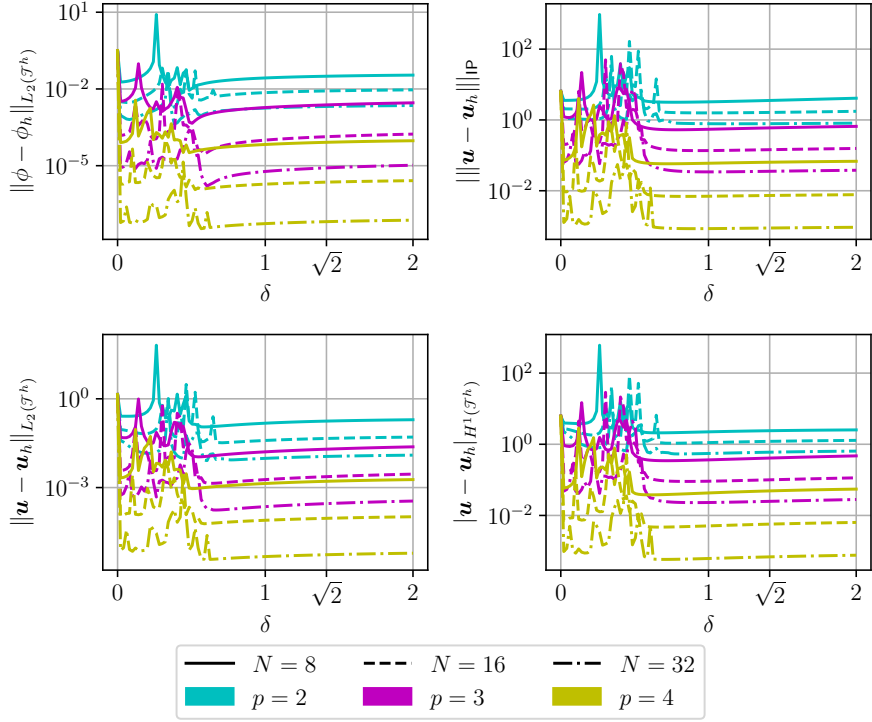


Figure 3: Measured error norms of the manufactured solution problem with varying parameter δ . Here we ensure the C^0 -RIPG scheme is stable with $\delta > \sqrt{2}$ as predicted in Section 4.1.

slip boundary conditions

$$\mathbf{u} \cdot \mathbf{n} = 0 \text{ on } \partial\Omega, \quad (48)$$

$$(2\mu\varepsilon(\mathbf{u}) \cdot \mathbf{n} - P\mathbf{n}) \cdot \boldsymbol{\tau} = 0 \text{ on } \partial\Omega. \quad (49)$$

For thermally driven buoyancy, we set

$$\mathbf{f} = \text{Ra}T \hat{\mathbf{y}}, \quad (50)$$

with viscosity model

$$\mu = \begin{cases} \mu_{\text{lin}} & \sigma_Y = 0, \\ 2(\mu_{\text{lin}}^{-1} + \mu_{\text{plast}}^{-1})^{-1} & \sigma_Y > 0, \end{cases} \quad (51)$$

$$\mu_{\text{lin}} = \exp(-\log(\Delta\mu_T)T + \log(\Delta\mu_z)z), \quad (52)$$

$$\mu_{\text{plast}} = 10^{-3} + \frac{\sigma_Y}{\sqrt{\varepsilon(\mathbf{u}) : \varepsilon(\mathbf{u})}}. \quad (53)$$

Here, $z = 1 - y$ is a measure of depth, Ra is the constant Rayleigh number and $\Delta\mu_T$, $\Delta\mu_z$ and σ_Y are constant viscosity model parameters to be defined in each benchmark case. The temperature

Case	Ra	$\Delta\mu_T$	$\Delta\mu_z$	σ_Y	Nu _{ref}	$u_{\text{rms,ref}}$
BB1a	10^4	1	1	0	4.884 409	42.864 947
BB2a	10^4	10^4	1	0	10.065 899	480.433 425
T2	10^2	10^5	1	1	8.559 459	140.775 535
T4	10^2	10^5	10	1	6.615 419	79.088 809

Table 1: Benchmark cases exhibited in Blankenbach et al. (1989) and Tosi et al. (2015) (BB and T prefixes, respectively) and corresponding reference values selected from those works.

field $T : \Omega \mapsto \mathbb{R}^+ \cup \{0\}$ satisfies the following advection–diffusion problem

$$\mathbf{u} \cdot \nabla T - \nabla^2 T = 0 \quad \text{in } \Omega, \quad (54)$$

$$T = 0 \quad \text{on } [0, 1] \times \{0\}, \quad (55)$$

$$T = 1 \quad \text{on } [0, 1] \times \{1\}, \quad (56)$$

$$\nabla T \cdot \mathbf{n} = 0 \quad \text{on } \{0, 1\} \times [0, 1]. \quad (57)$$

We discretize equations (54) to (57) using standard C^0 finite elements such that we seek $(\phi_h, T_h) \in V_0^{h,p} \times S^{h,p}$ such that equation (16) holds simultaneously with

$$(\mathbf{u}_h \cdot \nabla T_h, s_h) + (\nabla T_h, \nabla s_h) = 0 \quad (58)$$

for all $(\psi_h, s_h) \in V_0^{h,p} \times S_0^{h,p}$, where $S^{h,p} = \{v \in H^1(\Omega) : v|_\kappa \in \mathcal{P}_p(\kappa) \ \forall \kappa \in \mathcal{T}^h, \ v|_{[0,1] \times \{0\}} = 0, \ v|_{[0,1] \times \{1\}} = 1\}$ and $S_0^{h,p} = \{v \in H^1(\Omega) : v|_\kappa \in \mathcal{P}_p(\kappa) \ \forall \kappa \in \mathcal{T}^h, \ v|_{[0,1] \times \{0,1\}} = 0\}$.

In Table 1 we define a number of benchmark cases with corresponding Rayleigh numbers and viscosity models. The functionals of interest measured for comparison with the corresponding benchmark reports are as follows

$$\begin{aligned} \text{Nu} &= \int_0^1 (\nabla T_h \cdot \mathbf{n})|_{y=1} \, dx, & u_{\text{rms}} &= \sqrt{\int_\Omega \mathbf{u}_h^2 \, d\mathbf{x}}, \\ \langle W \rangle &= \sqrt{\int_\Omega T_h \mathbf{u}_h \cdot \hat{\mathbf{y}} \, d\mathbf{x}}, & \langle \Phi \rangle &= \sqrt{\int_\Omega 2\mu \varepsilon_h(\mathbf{u}_h) : \varepsilon_h(\mathbf{u}_h) \, d\mathbf{x}}, & \Delta &= \frac{\left| \langle W \rangle - \frac{\langle \Phi \rangle}{\text{Ra}} \right|}{\max\left(\langle W \rangle, \frac{\langle \Phi \rangle}{\text{Ra}}\right)}, \end{aligned}$$

where Nu is the Nusselt number at the top boundary, u_{rms} is the root mean square speed, $\langle W \rangle$ and $\langle \Phi \rangle$ are the average rates of work done against gravity and viscous dissipation, respectively, and Δ is a measure of thermal energy conservation. In Table 2 we tabulate the computed functional values from our implementation on a sequence of uniform triangular meshes for $p = 2, 3$.

In Figure 4 we compute errors in Nu and u_{rms} relative to the given reference values for the benchmark cases shown in Table 1. Here, the relative error measurement of computed quantity χ compared with reference value χ_{ref} is given by

$$\epsilon_{\text{ref}}(\chi) = \frac{|\chi - \chi_{\text{ref}}|}{\chi_{\text{ref}}}. \quad (59)$$

For the case BB1a (isoviscous model) we see that as the mesh is uniformly refined, the computed Nusselt number and root-mean-square velocity approximations, as compared with reference values, converge to zero at the rates $\mathcal{O}(h^{2(p-1)})$ and $\mathcal{O}(h^p)$ as h tends to zero, respectively,

Case	p	N	Nu	u_{rms}	$\langle W \rangle$	$\langle \Phi \rangle / \text{Ra}$	Δ
BB1a	2	8	5.159 790	41.877 692	3.812 435	3.721 304	$2.390\,357 \times 10^{-2}$
		16	5.015 557	42.613 520	3.866 134	3.841 287	$6.426\,728 \times 10^{-3}$
		32	4.923 947	42.801 576	3.879 774	3.873 409	$1.640\,653 \times 10^{-3}$
		64	4.894 819	42.849 068	3.883 246	3.881 644	$4.124\,164 \times 10^{-4}$
		128	4.887 047	42.860 973	3.884 118	3.883 717	$1.032\,472 \times 10^{-4}$
	3	8	4.997 386	42.859 417	3.883 614	3.894 593	$2.819\,064 \times 10^{-3}$
		16	4.894 932	42.864 517	3.884 342	3.887 360	$7.764\,650 \times 10^{-4}$
		32	4.885 120	42.864 918	3.884 405	3.885 177	$1.986\,228 \times 10^{-4}$
		64	4.884 454	42.864 943	3.884 409	3.884 603	$4.993\,627 \times 10^{-5}$
		128	4.884 412	42.864 945	3.884 409	3.884 458	$1.250\,158 \times 10^{-5}$
BB2a	2	8	11.569 494	494.791 616	10.639 110	9.866 476	$7.262\,202 \times 10^{-2}$
		16	10.731 001	487.372 110	9.151 660	8.917 624	$2.557\,305 \times 10^{-2}$
		32	10.306 838	483.106 619	9.101 327	9.018 523	$9.098\,057 \times 10^{-3}$
		64	10.129 296	481.246 438	9.072 895	9.046 327	$2.928\,342 \times 10^{-3}$
		128	10.081 744	480.619 011	9.067 279	9.059 942	$8.091\,935 \times 10^{-4}$
	3	8	11.039 987	481.181 654	9.217 020	9.258 907	$4.524\,017 \times 10^{-3}$
		16	10.225 818	481.626 650	9.107 274	9.123 698	$1.800\,123 \times 10^{-3}$
		32	10.073 773	480.583 438	9.064 849	9.072 503	$8.436\,236 \times 10^{-4}$
		64	10.066 181	480.403 057	9.065 588	9.067 885	$2.533\,984 \times 10^{-4}$
		128	10.065 910	480.427 513	9.065 872	9.066 485	$6.764\,788 \times 10^{-5}$
T2	2	8	8.670 484	130.718 863	7.175 272	7.024 771	$2.097\,492 \times 10^{-2}$
		16	8.852 719	135.810 284	7.405 343	7.330 546	$1.010\,052 \times 10^{-2}$
		32	8.677 987	139.186 405	7.514 772	7.477 494	$4.960\,578 \times 10^{-3}$
		64	8.587 873	140.198 404	7.542 252	7.528 339	$1.844\,703 \times 10^{-3}$
		128	8.565 231	140.580 896	7.553 466	7.548 985	$5.933\,286 \times 10^{-4}$
	3	8	9.044 719	137.032 238	7.479 251	7.480 751	$2.004\,897 \times 10^{-4}$
		16	8.622 321	140.017 268	7.533 352	7.536 932	$4.750\,446 \times 10^{-4}$
		32	8.557 657	140.503 070	7.550 360	7.552 252	$2.506\,208 \times 10^{-4}$
		64	8.557 513	140.702 836	7.557 034	7.557 831	$1.054\,292 \times 10^{-4}$
		128	8.559 291	140.769 772	7.559 261	7.559 543	$3.730\,833 \times 10^{-5}$
T4	2	8	6.964 560	76.225 863	5.486 364	5.347 143	$2.537\,569 \times 10^{-2}$
		16	6.879 954	78.177 425	5.583 371	5.521 602	$1.106\,295 \times 10^{-2}$
		32	6.702 668	78.807 864	5.604 996	5.583 245	$3.880\,586 \times 10^{-3}$
		64	6.637 644	78.990 505	5.611 148	5.604 410	$1.200\,818 \times 10^{-3}$
		128	6.620 866	79.060 030	5.614 094	5.612 224	$3.329\,760 \times 10^{-4}$
	3	8	6.931 491	78.787 124	5.613 935	5.617 167	$5.754\,950 \times 10^{-4}$
		16	6.651 302	79.002 440	5.610 692	5.614 473	$6.734\,658 \times 10^{-4}$
		32	6.615 929	79.045 743	5.612 879	5.614 332	$2.588\,058 \times 10^{-4}$
		64	6.615 222	79.082 175	5.615 025	5.615 510	$8.630\,228 \times 10^{-5}$
		128	6.615 397	79.088 264	5.615 384	5.615 517	$2.360\,951 \times 10^{-5}$

Table 2: Computed functional measurements from the numerical benchmark cases as computed with the C^0 -RIPG scheme.

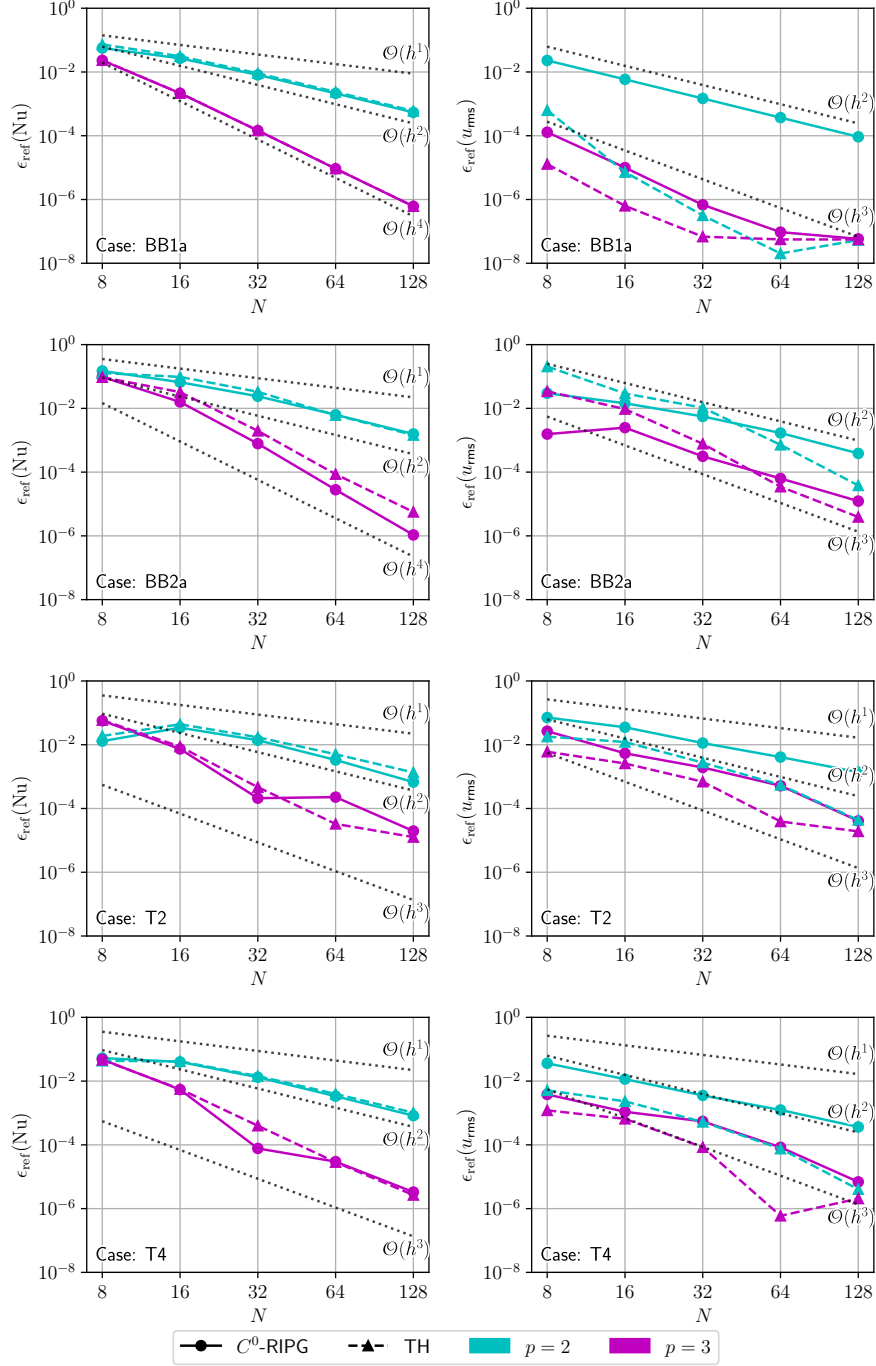


Figure 4: Measured functionals' errors relative to reference values selected from benchmark problems exhibited in Blankenbach et al. (1989); Tosi et al. (2015). We further compare the C^0 -RIPG formulation with a standard TH discretization.

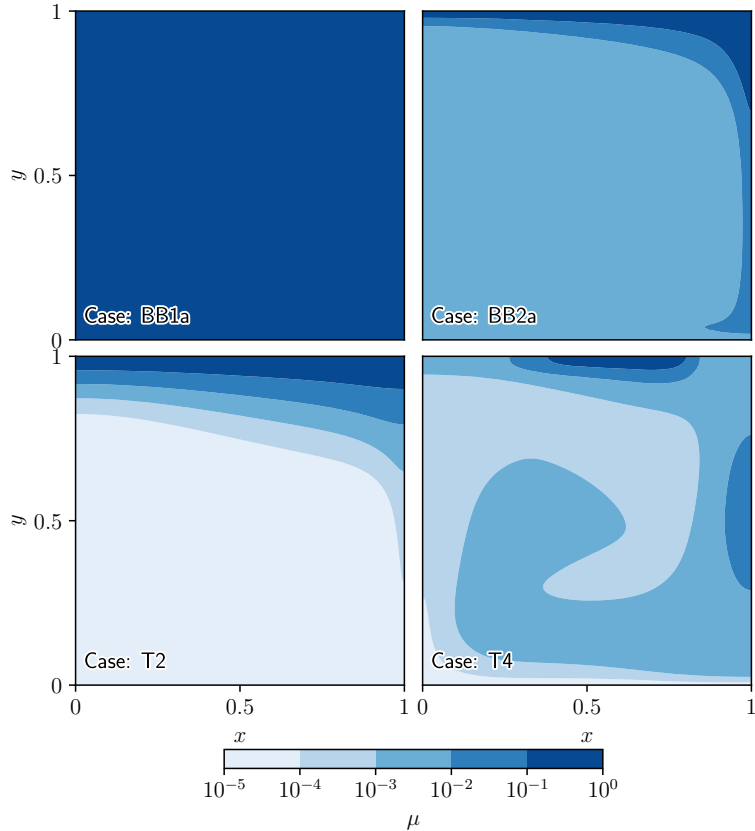


Figure 5: Viscosity fields as computed from the C^0 -RIPG discretization with $p = 3$ of the benchmark problems tabulated in Table 1. These fields are interpolated in the space $V_{\text{DG}}^{h,p=1}$ for visualization.

for $p = 2, 3$. However, we observe that when nonlinear viscosity models are employed, as in cases BB2a, T2 and T4, the order of convergence of these quantities of interest may be reduced; this is particularly evident for the ‘highly nonlinear’ cases T2 and T4 (cf. Figure 5).

Additionally, we compare the performance of the proposed C^0 -RIPG method with the TH discretization scheme which highlights the impact of employing an exactly divergence free velocity field approximation. When examining equivalent polynomial degrees in the underlying finite element spaces, we see that the C^0 -RIPG formulation yields a more precise Nusselt number approximation for fewer than half the number of degrees of freedom due to its solenoidal velocity field. This result is attained despite the fact that the root-mean-square velocity approximation of the C^0 -RIPG scheme is less accurate than that the corresponding quantity computed for the TH method for an equivalent polynomial degree. For the C^0 -RIPG method to yield a root-mean-square velocity approximation roughly equivalent to the TH method a polynomial degree one order higher should be employed.

Finally, we examine the balance of energy encapsulated by the functional Δ as tabulated in Table 2. Here, we see that energy is not exactly conserved. However, the values of Δ computed using the C^0 -RIPG scheme are comparable with the TH scheme results, $\Delta < 0.01\%$, reported in Tosi et al. (2015).

6 Concluding remarks

In this article we have presented the C^0 -RIPG formulation of the stream function formulation of the Stokes system with varying viscosity. We have shown that this scheme is stable provided the interior penalty parameter is selected so that $\delta > \sqrt{2}$. Moreover, our analysis and numerical experiments demonstrate that the scheme converges optimally with respect to uniform mesh refinement when the error is measured in an appropriate DG norm. Furthermore, the discretization provides an exactly divergence free approximation of the velocity which, in the context of numerical benchmarks of mantle convection simulations, yields a more precise approximation of the advected temperature field. Our implementation is available in Sime (2023) for use with the FEniCSx library.

7 Acknowledgments

This research was partly supported by NSF-EAR grant 2021027. N. Sime gratefully acknowledges the support of Carnegie Institution for Science President's Fellowship.

A C^0 -RIPG formulation derivation

In this appendix we outline the derivation of the proposed C^0 -RIPG scheme (16); to this end we first develop the SIPG DG discretization of the problem in equations (1) to (4), then consider the restriction to the H^1 -conforming FE space $V^{h,p}$.

A.1 Flux formulation

For completeness, we consider the following generalized stream function formulation of equation (1) with corresponding boundary conditions:

$$\nabla \times \left(-\nabla \cdot (2\mu\varepsilon(\nabla \times \phi) - P\mathbb{I}) \right) = \nabla \times \mathbf{f} \quad \text{in } \Omega, \quad (60)$$

$$\phi = \phi_D \quad \text{on } \partial\Omega_{\phi,D} \quad (61)$$

$$\nabla \times \phi = \mathbf{u}_D \quad \text{on } \partial\Omega_D, \quad (62)$$

$$(2\mu\varepsilon(\nabla \times \phi) - P\mathbb{I}) \cdot \mathbf{n} = \mathbf{g}_N \quad \text{on } \partial\Omega_N, \quad (63)$$

$$\left(-\nabla \cdot (2\mu\varepsilon(\nabla \times \phi) - P\mathbb{I}) \right) \times \mathbf{n} = \mathbf{f} \times \mathbf{n} \quad \text{on } \partial\Omega_{\phi,N}. \quad (64)$$

Here, \mathbb{I} is the identity tensor and the exterior boundary is split into components for the stream function and velocity boundary conditions such that $\partial\Omega = \partial\Omega_{\phi,D} \cup \partial\Omega_{\phi,N}$ and $\partial\Omega = \partial\Omega_D \cup \partial\Omega_N$ where the boundary components do not overlap, $\partial\Omega_{\phi,D} \cap \partial\Omega_{\phi,N} = \emptyset$ and $\partial\Omega_D \cap \partial\Omega_N = \emptyset$. We define the rank 4 tensor $G = \partial(2\mu\varepsilon(\mathbf{u}))/\partial(\nabla\mathbf{u})$; given $\sigma \in \mathbb{R}^{2 \times 2}$, its product and transpose product are defined, respectively, by

$$G\sigma = G_{ijkl}\sigma_{ij} \quad \text{and} \quad G^\top\sigma = G_{ijkl}\sigma_{kl}, \quad (65)$$

such that $2\mu\varepsilon(\mathbf{u}) = G\nabla\mathbf{u}$. Let $F_1 : \Omega \mapsto \mathbb{R}^2$, $F_2 : \Omega \mapsto \mathbb{R}^{2 \times 2}$ and $F_3 : \Omega \mapsto \mathbb{R}^2$ such that we recast equation (60) in terms of four first order equations

$$\nabla \times \mathbf{f} = \nabla \times F_1, \quad F_1 = -\nabla \cdot F_2, \quad F_2 = G\nabla F_3 - P\mathbb{I}, \quad F_3 = \nabla \times \phi, \quad (66)$$

where it is evident that

$$F_1(\phi) = -\nabla \cdot (2\mu\varepsilon(\nabla \times \phi) - P\mathbb{I}) \quad \text{and} \quad F_2(\phi) = 2\mu\varepsilon(\nabla \times \phi) - P\mathbb{I}. \quad (67)$$

We multiply each equation in (66) by $v_1 : \Omega \mapsto \mathbb{R}$, $\mathbf{v}_2 : \Omega \mapsto \mathbb{R}^2$, $v_3 : \Omega \mapsto \mathbb{R}^{2 \times 2}$ and $\mathbf{v}_4 : \Omega \mapsto \mathbb{R}^2$, respectively, and integrate over an element $\kappa \in \mathcal{T}^h$ to give

$$(\nabla \times \mathbf{f}, v_1)_\kappa = (\nabla \times F_1, v_1)_\kappa, \quad (68)$$

$$(F_1, \mathbf{v}_2)_\kappa = (-\nabla \cdot F_2, \mathbf{v}_2)_\kappa, \quad (69)$$

$$(F_2, v_3)_\kappa = (G\nabla F_3, v_3)_\kappa - (P\mathbb{I}, v_3)_\kappa, \quad (70)$$

$$(F_3, \mathbf{v}_4)_\kappa = (\nabla \times \phi, \mathbf{v}_4)_\kappa. \quad (71)$$

Integrating by parts equations (68) to (70) once, and given the lack of prescribed boundary data, equation (71) twice, we deduce that

$$(\nabla \times \mathbf{f}, v_1)_\kappa = (F_1, \nabla \times v_1)_\kappa - \langle \widehat{F}_1, \mathbf{n} \times v_1 \rangle_{\partial\kappa}, \quad (72)$$

$$(F_1, \mathbf{v}_2)_\kappa = (F_2, \nabla \mathbf{v}_2)_\kappa - \langle \widehat{F}_2, \mathbf{v}_2 \otimes \mathbf{n} \rangle_{\partial\kappa}, \quad (73)$$

$$(F_2, v_3)_\kappa = -(F_3, \nabla \cdot (G^\top v_3))_\kappa + \langle \widehat{F}_3 \otimes \mathbf{n}, G^\top v_3 \rangle_{\partial\kappa} - (P\mathbb{I}, v_3)_\kappa, \quad (74)$$

$$(F_3, \mathbf{v}_4)_\kappa = (\nabla \times \phi, \mathbf{v}_4)_\kappa - \langle \widehat{\phi} - \phi, \mathbf{n} \times \mathbf{v}_4 \rangle_{\partial\kappa}, \quad (75)$$

where $\langle \widehat{\cdot} \rangle_{\partial\kappa}$ indicates a consistent and conservative flux approximation. We now proceed to eliminate the additional auxiliary variables introduced in order to derive the so-called flux formulation. To this end, we first select $\mathbf{v}_4 = \nabla \cdot (G^\top v_3)$; inserting equation (75) into equation (74) yields

$$(F_2, v_3)_\kappa = -(\nabla \times \phi, \nabla \cdot (G^\top v_3))_\kappa + \langle \widehat{\phi} - \phi, \mathbf{n} \times (\nabla \cdot (G^\top v_3)) \rangle_{\partial\kappa} + \langle \widehat{F}_3 \otimes \mathbf{n}, G^\top v_3 \rangle_{\partial\kappa} - (P\mathbb{I}, v_3)_\kappa. \quad (76)$$

Given a lack of prescribed boundary information regarding F_3 we integrate the first term in equation (76) by parts again giving

$$(F_2, v_3)_\kappa = (\nabla(\nabla \times \phi), G^\top v_3)_\kappa + \langle \widehat{\phi} - \phi, \mathbf{n} \times (\nabla \cdot (G^\top v_3)) \rangle_{\partial\kappa} + \langle (\widehat{F}_3 - \nabla \times \phi) \otimes \mathbf{n}, G^\top v_3 \rangle_{\partial\kappa} - (P\mathbb{I}, v_3)_\kappa. \quad (77)$$

Let $\mathbf{v}_2 = \nabla \times v_1$, then inserting equation (73) into equation (72) yields

$$(\nabla \times \mathbf{f}, v_1)_\kappa = (F_2, \nabla(\nabla \times v_1))_\kappa - \langle \widehat{F}_2, (\nabla \times v_1) \otimes \mathbf{n} \rangle_{\partial\kappa} - \langle \widehat{F}_1, \mathbf{n} \times v_1 \rangle_{\partial\kappa}. \quad (78)$$

Next we set $v_3 = \nabla(\nabla \times v_1)$; substituting equation (77) into equation (78) and summing over all elements in the mesh \mathcal{T}^h gives

$$\begin{aligned} \sum_{\kappa \in \mathcal{T}^h} (\nabla \times \mathbf{f}, v_1)_\kappa &= \sum_{\kappa \in \mathcal{T}^h} (\nabla(\nabla \times \phi), G^\top \nabla(\nabla \times v_1))_\kappa - \sum_{\kappa \in \mathcal{T}^h} (P\mathbb{I}, \nabla(\nabla \times v_1))_\kappa \\ &\quad + \sum_{\kappa \in \mathcal{T}^h} \langle \widehat{\phi} - \phi, \mathbf{n} \times (\nabla \cdot (G^\top \nabla(\nabla \times v_1))) \rangle_{\partial\kappa} \\ &\quad + \sum_{\kappa \in \mathcal{T}^h} \langle (\widehat{F}_3 - \nabla \times \phi) \otimes \mathbf{n}, G^\top \nabla(\nabla \times v_1) \rangle_{\partial\kappa} \\ &\quad - \sum_{\kappa \in \mathcal{T}^h} \langle \widehat{F}_2, (\nabla \times v_1) \otimes \mathbf{n} \rangle_{\partial\kappa} \\ &\quad - \sum_{\kappa \in \mathcal{T}^h} \langle \widehat{F}_1, \mathbf{n} \times v_1 \rangle_{\partial\kappa}. \end{aligned} \quad (79)$$

Finally, given

$$(P\mathbb{I}, \nabla(\nabla \times v_1))_\kappa = (P, \nabla \cdot (\nabla \times v_1))_\kappa = 0 \quad (80)$$

and replacing the flux approximations with their corresponding Neumann boundary data on $\partial\Omega_N$ and $\partial\Omega_{\phi,N}$, as well as the analytical solution with the (DG) finite element approximation $\phi_h \in V_{\text{DG}}^{h,p} = \{v \in L_2(\Omega) : v|_\kappa \in \mathcal{P}_p(\kappa) \ \forall \kappa \in \mathcal{T}^h\}$, $p \geq 2$, and selecting $v_1 = \psi$ gives rise to the flux formulation: find $\phi_h \in V_{\text{DG}}^{h,p}$ such that

$$\begin{aligned} \sum_{\kappa \in \mathcal{T}^h} (\nabla \times \mathbf{f}, \psi)_\kappa &= \sum_{\kappa \in \mathcal{T}^h} (\nabla(\nabla \times \phi_h), G^\top \nabla(\nabla \times \psi))_\kappa \\ &\quad - \sum_{\kappa \in \mathcal{T}^h} \langle \mathbf{f} \times \mathbf{n}, \psi \rangle_{\partial\kappa \cap \partial\Omega_{\phi,N}} - \sum_{\kappa \in \mathcal{T}^h} \langle \mathbf{g}_N, \nabla \times \psi \rangle_{\partial\kappa \cap \partial\Omega_N} \\ &\quad + \sum_{\kappa \in \mathcal{T}^h} \langle \widehat{\phi}_h - \phi_h, \mathbf{n} \times (\nabla \cdot (G^\top \nabla(\nabla \times \psi))) \rangle_{\partial\kappa \setminus \partial\Omega_{\phi,N}} \\ &\quad + \sum_{\kappa \in \mathcal{T}^h} \langle (\widehat{F}_3 - \nabla \times \phi_h) \otimes \mathbf{n}, G^\top \nabla(\nabla \times \psi) \rangle_{\partial\kappa \setminus \partial\Omega_N} \\ &\quad - \sum_{\kappa \in \mathcal{T}^h} \langle \widehat{F}_2, (\nabla \times \psi) \otimes \mathbf{n} \rangle_{\partial\kappa \setminus \partial\Omega_N} \\ &\quad - \sum_{\kappa \in \mathcal{T}^h} \langle \widehat{F}_1, \mathbf{n} \times \psi \rangle_{\partial\kappa \setminus \partial\Omega_{\phi,N}} \quad \forall \psi \in V_{\text{DG}}^{h,p}. \end{aligned} \quad (81)$$

A.2 Primal formulation

We define the specialized average operators

$$\{\cdot\}_\ell|_F = \ell^+(\cdot)^+ + \ell^-(\cdot)^- \quad \text{and} \quad \{\cdot\}_{\ell^\mp}|_F = \ell^-(\cdot)^+ + \ell^+(\cdot)^- \quad F \in \Gamma_I, \quad (82)$$

where the weights are constrained by $\ell^+ + \ell^- = 1$; the relationship to the weights w^\pm will become evident below. For sufficiently smooth vector and scalar valued functions \mathbf{v} and q , respectively, we define the following jump operators

$$\begin{aligned} [\mathbf{v}]|_F &= \mathbf{n}^+ \cdot \mathbf{v}^+ + \mathbf{n}^- \cdot \mathbf{v}^-, & F \in \Gamma_I, \\ [\mathbf{v}]_\times|_F &= \mathbf{n}^+ \times \mathbf{v}^+ + \mathbf{n}^- \times \mathbf{v}^-, & F \in \Gamma_I, \\ [q]|_F &= \mathbf{n}^+ q^+ + \mathbf{n}^- q^-, & F \in \Gamma_I. \end{aligned}$$

Lemma A.1. *For sufficiently smooth $q : \Omega \mapsto \mathbb{R}$, $\mathbf{v}, \mathbf{z} : \Omega \mapsto \mathbb{R}^2$ and $\sigma : \Omega \mapsto \mathbb{R}^{2 \times 2}$, the following identities hold*

$$\sum_{\kappa \in \mathcal{T}^h} \langle q, \mathbf{v} \cdot \mathbf{n} \rangle_{\partial\kappa} = \langle [q], \{\mathbf{v}\}_{\ell^\mp} \rangle_{\Gamma_I} + \langle \{\{q\}\}_\ell, [\mathbf{v}] \rangle_{\Gamma_I} + \langle q\mathbf{n}, \mathbf{v} \rangle_{\partial\Omega}, \quad (83)$$

$$\sum_{\kappa \in \mathcal{T}^h} \langle \sigma, \mathbf{v} \otimes \mathbf{n} \rangle_{\partial\kappa} = \langle [\mathbf{v}]_\otimes, \{\{\sigma\}\}_{\ell^\mp} \rangle_{\Gamma_I} + \langle \{\{\mathbf{v}\}\}_\ell, [\sigma] \rangle_{\Gamma_I} + \langle \mathbf{v} \otimes \mathbf{n}, \sigma \rangle_{\partial\Omega}, \quad (84)$$

$$\sum_{\kappa \in \mathcal{T}^h} \langle \mathbf{z}, \mathbf{n} \times \mathbf{v} \rangle_{\partial\kappa} = \langle [\mathbf{v}]_\times, \{\{\mathbf{z}\}\}_{\ell^\mp} \rangle_{\Gamma_I} - \langle \{\{\mathbf{v}\}\}_\ell, [\mathbf{z}]_\times \rangle_{\Gamma_I} + \langle \mathbf{n} \times \mathbf{v}, \mathbf{z} \rangle_{\partial\Omega}. \quad (85)$$

Proof. Consider equation (83). In the absence of interior mesh facets, on the boundary it is clear that equation (83) trivially holds, i.e.,

$$\sum_{\kappa \in \mathcal{T}^h} \langle q, \mathbf{v} \cdot \mathbf{n} \rangle_{\partial\kappa \cap \partial\Omega} = \langle q\mathbf{n}, \mathbf{v} \rangle_{\partial\Omega}.$$

Let us now consider the interior mesh facets; to this end the left-hand side of equation (83) may be rewritten as follows

$$\sum_{\kappa \in \mathcal{T}^h} \langle q, \mathbf{v} \cdot \mathbf{n} \rangle_{\partial\kappa \setminus \partial\Omega} = \langle q^+, \mathbf{v}^+ \cdot \mathbf{n}^+ \rangle_{\Gamma_I} + \langle q^-, \mathbf{v}^- \cdot \mathbf{n}^- \rangle_{\Gamma_I}.$$

Using the fact that $1 = \ell^+ + \ell^-$, we get

$$\begin{aligned} \sum_{\kappa \in \mathcal{T}^h} \langle q, \mathbf{v} \cdot \mathbf{n} \rangle_{\partial\kappa \setminus \partial\Omega} &= \langle \ell^+ q^+, \mathbf{v}^+ \cdot \mathbf{n}^+ \rangle_{\Gamma_I} + \langle \ell^- q^+, \mathbf{v}^+ \cdot \mathbf{n}^+ \rangle_{\Gamma_I} + \langle \ell^+ q^-, \mathbf{v}^- \cdot \mathbf{n}^- \rangle_{\Gamma_I} \\ &\quad + \langle \ell^- q^-, \mathbf{v}^- \cdot \mathbf{n}^- \rangle_{\Gamma_I}. \end{aligned}$$

Noting that on an interior mesh facet we have $q^+ \mathbf{v}^- \cdot \mathbf{n}^+ + q^+ \mathbf{v}^- \cdot \mathbf{n}^- = 0$ and $q^- \mathbf{v}^+ \cdot \mathbf{n}^+ + q^- \mathbf{v}^+ \cdot \mathbf{n}^- = 0$, then

$$\begin{aligned} \sum_{\kappa \in \mathcal{T}^h} \langle q, \mathbf{v} \cdot \mathbf{n} \rangle_{\partial\kappa \setminus \partial\Omega} &= \langle \ell^+ q^+, \mathbf{v}^+ \cdot \mathbf{n}^+ \rangle_{\Gamma_I} + \langle \ell^- q^+, \mathbf{v}^+ \cdot \mathbf{n}^+ \rangle_{\Gamma_I} + \langle \ell^+ q^-, \mathbf{v}^- \cdot \mathbf{n}^- \rangle_{\Gamma_I} + \langle \ell^- q^-, \mathbf{v}^- \cdot \mathbf{n}^- \rangle_{\Gamma_I} \\ &\quad + \langle \ell^+ q^+, \mathbf{v}^- \cdot \mathbf{n}^+ \rangle_{\Gamma_I} + \langle \ell^- q^+, \mathbf{v}^- \cdot \mathbf{n}^+ \rangle_{\Gamma_I} + \langle \ell^+ q^-, \mathbf{v}^+ \cdot \mathbf{n}^- \rangle_{\Gamma_I} + \langle \ell^- q^-, \mathbf{v}^+ \cdot \mathbf{n}^- \rangle_{\Gamma_I} \\ &\quad + \langle \ell^+ q^-, \mathbf{v}^+ \cdot \mathbf{n}^+ \rangle_{\Gamma_I} + \langle \ell^- q^-, \mathbf{v}^+ \cdot \mathbf{n}^+ \rangle_{\Gamma_I} + \langle \ell^+ q^-, \mathbf{v}^- \cdot \mathbf{n}^- \rangle_{\Gamma_I} + \langle \ell^- q^-, \mathbf{v}^- \cdot \mathbf{n}^- \rangle_{\Gamma_I}. \end{aligned}$$

Collecting coefficients of $\mathbf{v}^+ \cdot \mathbf{n}^+$ and $\mathbf{v}^- \cdot \mathbf{n}^-$ gives

$$\begin{aligned} \sum_{\kappa \in \mathcal{T}^h} \langle q, \mathbf{v} \cdot \mathbf{n} \rangle_{\partial\kappa \setminus \partial\Omega} &= \langle \{\{q\}\}_\ell, [\mathbf{v}] \rangle_{\Gamma_I} \\ &\quad + \langle \ell^- q^+, \mathbf{v}^+ \cdot \mathbf{n}^+ \rangle_{\Gamma_I} + \langle \ell^+ q^-, \mathbf{v}^- \cdot \mathbf{n}^- \rangle_{\Gamma_I} \\ &\quad + \langle \ell^+ q^+, \mathbf{v}^- \cdot \mathbf{n}^+ \rangle_{\Gamma_I} + \langle \ell^- q^+, \mathbf{v}^- \cdot \mathbf{n}^+ \rangle_{\Gamma_I} + \langle \ell^- q^+, \mathbf{v}^- \cdot \mathbf{n}^- \rangle_{\Gamma_I} \\ &\quad + \langle \ell^+ q^-, \mathbf{v}^+ \cdot \mathbf{n}^+ \rangle_{\Gamma_I} + \langle \ell^+ q^-, \mathbf{v}^+ \cdot \mathbf{n}^- \rangle_{\Gamma_I} + \langle \ell^- q^-, \mathbf{v}^+ \cdot \mathbf{n}^- \rangle_{\Gamma_I}. \end{aligned}$$

If we now collect coefficients of $q^+ \mathbf{n}^+$ and $q^- \mathbf{n}^-$, we get

$$\begin{aligned} \sum_{\kappa \in \mathcal{T}^h} \langle q, \mathbf{v} \cdot \mathbf{n} \rangle_{\partial\kappa \setminus \partial\Omega} &= \langle \{\{q\}\}_\ell, [\mathbf{v}] \rangle_{\Gamma_I} + \langle \{\{\mathbf{v}\}\}_{\ell^\mp}, [q] \rangle_{\Gamma_I} \\ &\quad + \langle \ell^- q^+, \mathbf{v}^- \cdot \mathbf{n}^+ \rangle_{\Gamma_I} + \langle \ell^- q^+, \mathbf{v}^- \cdot \mathbf{n}^- \rangle_{\Gamma_I} + \langle \ell^+ q^-, \mathbf{v}^+ \cdot \mathbf{n}^+ \rangle_{\Gamma_I} + \langle \ell^+ q^-, \mathbf{v}^+ \cdot \mathbf{n}^- \rangle_{\Gamma_I}, \\ &= \langle \{\{q\}\}_\ell, [\mathbf{v}] \rangle_{\Gamma_I} + \langle \{\{\mathbf{v}\}\}_{\ell^\mp}, [q] \rangle_{\Gamma_I}. \end{aligned}$$

Noting that $\langle \mathbf{z}, \mathbf{n} \times \mathbf{v} \rangle_{\partial\kappa \setminus \partial\Omega} = -\langle \mathbf{n} \times \mathbf{z}, \mathbf{v} \rangle_{\partial\kappa \setminus \partial\Omega}$ equations (84) and (85) follow analogously. \square

Employing the identities in equations (83) to (85), equation (81) may be rewritten in the following equivalent manner

$$\begin{aligned}
& (\nabla_h \times \mathbf{f}, \psi)_\Omega \\
&= (\nabla_h(\nabla_h \times \phi_h), G^\top \nabla_h(\nabla_h \times \psi))_\Omega - \langle \mathbf{f} \times \mathbf{n}, \psi \rangle_{\partial\Omega_{\phi,N}} - \langle \mathbf{g}_N, \nabla \times \psi \rangle_{\partial\Omega_N} \\
&+ \langle \{\widehat{\phi}_h - \phi_h\}_{\ell^\mp}, \llbracket \nabla_h \cdot (G^\top \nabla_h(\nabla_h \times \psi)) \rrbracket_\times \rangle_{\Gamma_I} \\
&- \langle \llbracket \widehat{\phi}_h - \phi_h \rrbracket_\times, \{\nabla_h \cdot (G^\top \nabla_h(\nabla_h \times \psi))\}_{\ell} \rangle_{\Gamma_I} \\
&+ \langle \widehat{\phi}_h - \phi_h, \mathbf{n} \times \nabla_h \cdot (G^\top \nabla_h(\nabla_h \times \psi)) \rangle_{\partial\Omega_{\phi,D}} \\
&+ \langle \llbracket \widehat{F}_3 - \nabla_h \times \phi_h \rrbracket_\otimes, \{\{G^\top \nabla_h(\nabla_h \times \psi)\}_{\ell^\mp}\}_{\ell} \rangle_{\Gamma_I} \\
&+ \langle \{\widehat{F}_3 - \nabla_h \times \phi_h\}_{\ell}, \llbracket G^\top \nabla_h(\nabla_h \times \psi) \rrbracket \rangle_{\Gamma_I} \\
&+ \langle (\widehat{F}_3 - \nabla_h \times \phi_h) \otimes \mathbf{n}, G^\top \nabla_h(\nabla_h \times \psi) \rangle_{\partial\Omega_D} \\
&- \langle \{\widehat{F}_2\}_{\ell^\mp}, \llbracket \nabla_h \times \psi \rrbracket_\otimes \rangle_{\Gamma_I} - \langle \llbracket \widehat{F}_2 \rrbracket, \{\nabla_h \times \psi\}_{\ell} \rangle_{\Gamma_I} - \langle \widehat{F}_2, (\nabla_h \times \psi) \otimes \mathbf{n} \rangle_{\partial\Omega_D} \\
&- \langle \{\widehat{F}_1\}_{\ell^\mp}, \llbracket \psi \rrbracket_\times \rangle_{\partial\Omega_{\phi,D}} + \langle \llbracket \widehat{F}_1 \rrbracket_\times, \{\psi\}_{\ell} \rangle_{\Gamma_I} - \langle \widehat{F}_1, \mathbf{n} \times \psi \rangle_{\partial\Omega_{\phi,D}}. \tag{86}
\end{aligned}$$

A.3 SIPG formulation

The choice of the flux approximations profoundly affects the numerical properties of the method (Arnold et al., 2001). We choose the flux approximations \widehat{F}_1 , \widehat{F}_2 and \widehat{F}_3 and $\widehat{\phi}_h$ according to the SIPG formulation such that

$$\widehat{F}_1 = \begin{cases} \{\{F_1(\phi_h)\}_{\ell} - \alpha \llbracket \phi_h \rrbracket_\times & \text{on } \Gamma_I, \\ F_1(\phi) - \alpha \mathbf{n} \times (\phi_h - \phi_D) & \text{on } \partial\Omega_{\phi,D}, \end{cases} \tag{87}$$

$$\widehat{F}_2 = \begin{cases} \{\{F_2(\nabla \times \phi_h)\}_{\ell^\mp} - \beta \llbracket \nabla \times \phi_h \rrbracket_\otimes & \text{on } \Gamma_I, \\ F_2(\nabla \times \phi_h) - \beta (\nabla \times \phi_h - \mathbf{u}_D) \otimes \mathbf{n} & \text{on } \partial\Omega_D, \end{cases} \tag{88}$$

$$\widehat{F}_3 = \begin{cases} \{\{F_3(\nabla \times \phi_h)\}_{\ell} & \text{on } \Gamma_I, \\ F_3(\mathbf{u}_D) & \text{on } \partial\Omega_D, \end{cases} \tag{89}$$

$$\widehat{\phi}_h = \begin{cases} \{\phi_h\}_{\ell^\mp} & \text{on } \Gamma_I, \\ \phi_D & \text{on } \partial\Omega_{\phi,D}, \end{cases} \tag{90}$$

Here, the terms α and β are penalty parameters required to ensure stability of the underlying method. Inserting the flux functions in equations (87) to (90) into equation (86) we arrive at the facet oriented formulation: find $\phi_h \in V_{\text{DG}}^{h,p}$ such that

$$\begin{aligned}
& (\nabla_h \times \mathbf{f}, \psi)_\Omega = (\nabla_h(\nabla_h \times \phi_h), G^\top \nabla_h(\nabla_h \times \psi))_\Omega \\
&- \langle \mathbf{f} \times \mathbf{n}, \psi \rangle_{\partial\Omega_{\phi,N}} - \langle \mathbf{g}_N, \nabla_h \times \psi \rangle_{\partial\Omega_N} \\
&+ \langle \phi_D - \phi_h, \mathbf{n} \times \nabla_h \cdot (G^\top \nabla_h(\nabla_h \times \psi)) \rangle_{\partial\Omega_{\phi,D}} + \langle \llbracket \phi_h \rrbracket_\times, \{\nabla_h \cdot (G^\top \nabla_h(\nabla_h \times \psi))\}_{\ell} \rangle_{\Gamma_I} \\
&+ \langle (\mathbf{u}_D - \nabla_h \times \phi_h) \otimes \mathbf{n}, G^\top \nabla_h(\nabla_h \times \psi) \rangle_{\partial\Omega_D} - \langle \llbracket \nabla_h \times \phi_h \rrbracket_\otimes, \{\{G^\top \nabla_h(\nabla_h \times \psi)\}_{\ell^\mp}\}_{\ell} \rangle_{\Gamma_I} \\
&- \langle \{\{2\mu\varepsilon_h(\nabla_h \times \phi_h)\}_{\ell^\mp} - \beta \llbracket \nabla_h \times \phi_h \rrbracket_\otimes, \llbracket \nabla_h \times \psi \rrbracket_\otimes \rangle_{\Gamma_I} \\
&- \langle 2\mu\varepsilon_h(\nabla_h \times \phi_h) - \beta (\nabla_h \times \phi_h - \mathbf{u}_D) \otimes \mathbf{n}, (\nabla_h \times \psi) \otimes \mathbf{n} \rangle_{\partial\Omega_D} \\
&- \langle \{-\nabla_h \cdot (2\mu\varepsilon_h(\nabla_h \times \phi_h))\}_{\ell} - \alpha \llbracket \phi_h \rrbracket_\times, \llbracket \psi \rrbracket_\times \rangle_{\Gamma_I} \\
&- \langle -\nabla_h \cdot (2\mu\varepsilon_h(\nabla_h \times \phi_h)) - \alpha \mathbf{n} \times (\phi_h - \phi_D), \mathbf{n} \times \psi \rangle_{\partial\Omega_{\phi,D}} \quad \forall \psi \in V_{\text{DG}}^{h,p}. \tag{91}
\end{aligned}$$

A.4 C^0 -IPG formulation

In order to reduce equation (91) to the C^0 -IPG formulation we restrict the space in which the FE solution is sought to $V_0^{h,p}$. Note that given the C^0 continuity of a function $\psi_h \in V_0^{h,p}$ we have $([\![\psi_h]\!]_{\otimes})_{ij} = 0$, $[\![\psi_h]\!]_{\times} = \mathbf{0}$ and $\psi_h|_{\partial\Omega_D} = 0$. Furthermore we notice that for isotropic viscosity we have $2\mu\varepsilon(\mathbf{u}) = G\nabla\mathbf{u} = G^T\nabla\mathbf{u}$, where

$$G = \mu \begin{pmatrix} \begin{pmatrix} 2 & 0 \\ 0 & 0 \\ 0 & 1 \\ 1 & 0 \end{pmatrix} & \begin{pmatrix} 0 & 1 \\ 1 & 0 \\ 0 & 0 \\ 0 & 2 \end{pmatrix} \end{pmatrix}, \quad (92)$$

and integrating by parts the left side we have

$$(\nabla_h \times \mathbf{f}, \psi) = (\mathbf{f}, \nabla_h \times \psi) - \langle \mathbf{f} \times \mathbf{n}, \psi \rangle_{\partial\Omega_{\phi,N}}. \quad (93)$$

Eliminating these terms from the facet oriented formulation in equation (91), setting $w^{\pm} = \ell^{\mp}$ (i.e., $\{\!\{ \cdot \}\!\} = \{\!\{ \cdot \}\!\}_{\ell^{\mp}}$), substituting for $\mathbf{u}_h = \nabla_h \times \phi_h$ and $\mathbf{v}_h = \nabla_h \times \psi_h$ and rearranging for bilinear and linear components we arrive at the formulation in equations (16), (17) and (19).

Acronyms

DG discontinuous Galerkin

FE finite element

HDG hybrid discontinuous Galerkin

IPG interior penalty Galerkin

PDE partial differential equation

RIPG robust interior penalty Galerkin

SIPG symmetric interior penalty Galerkin

TH Taylor–Hood

UFL Unified Form Language

References

- M. S. Alnæs, A. Logg, K. B. Ølgaard, M. E. Rognes, and G. N. Wells. Unified Form Language: A domain-specific language for weak formulations of partial differential equations. *ACM Transactions on Mathematical Software*, 40:9:1–9:37, 2014.
- J. H. Argyris, I. Fried, and D. W. Scharpf. The TUBA family of plate elements for the matrix displacement method. *The Aeronautical Journal*, 72(692):701–709, 1968.
- D. N. Arnold, F. Brezzi, B. Cockburn, and L. Marini. Unified analysis of discontinuous Galerkin methods for elliptic problems. *SIAM Journal on Numerical Analysis*, 39:1749–1779, 2001.

- D. Bercovici. Mantle dynamics: An introduction and overview. In G. Schubert, editor, *Treatise on Geophysics (2nd edition), Volume 7 "Mantle Dynamics" (Bercovici, D (ed.)) pp 1–22*. Elsevier, Amsterdam, The Netherlands, 2015. doi: 10.1016/B978-0-444-53802-4.00132-9.
- B. Blankenbach, F. Busse, U. Christensen, L. Cserepes, D. Gunkel, U. Hansen, H. Harder, G. Jarvis, M. Koch, G. Marquart, D. Moore, P. Olson, H. Schmeling, and T. Schnaubelt. A benchmark comparison for mantle convection codes. *Geophysical Journal International*, 98: 23–38, 1989. doi: 10.1111/j.1365-246X.1989.tb05511.x.
- A. Bossman and P. E. van Keken. Dynamics of plumes in a compressible mantle with phase changes: Implications for phase change boundary topography. *Physics of the Earth and Planetary Interiors*, 224:21–31, 2013. doi: 10.1016/j.pepi.2013.09.002.
- J. P. Brandenburg, E. H. Hauri, P. E. van Keken, and C. J. Ballentine. A multiple-system study of the geochemical evolution of the mantle with force-balanced plates and thermochemical effects. *Earth and Planetary Science Letters*, 276:1–13, 2008.
- F. Brezzi, J. Douglas, and L. D. Marini. Two families of mixed finite elements for second order elliptic problems. *Numerische Mathematik*, 47:217–235, 1985.
- A. Chernov. Optimal convergence estimates for the trace of the polynomial l^2 -projection operator on a simplex. *Mathematics of Computation*, 81(278):765–787, 2012.
- U. R. Christensen and A. W. Hofmann. Segregation of subducted oceanic crust in the convecting mantle. *Journal of Geophysical Research*, 99:19867–19884, 1994. doi: 10.1029/93JB03403.
- B. Cockburn, J. Gopalakrishnan, N. Nguyen, J. Peraire, and F.-J. Sayas. Analysis of HDG methods for Stokes flow. *Mathematics of Computation*, 80(274):723–760, 2011.
- Z. Dong and E. H. Georgoulis. Robust interior penalty discontinuous Galerkin methods. *Journal of Scientific Computing*, 92(2):57, 2022.
- Z. Dong and L. Mascotto. hp -optimal interior penalty discontinuous Galerkin methods for the biharmonic problem. *Journal of Scientific Computing*, 96(1):30, 2023. doi: 10.1007/s10915-023-02253-y.
- G. Engel, K. Garikipati, T. J. R. Hughes, M. G. Larson, L. Mazzei, and R. L. Taylor. Continuous/discontinuous finite element approximations of fourth-order elliptic problems in structural and continuum mechanics with applications to thin beams and plates, and strain gradient elasticity. *Computer Methods in Applied Mechanics and Engineering*, 191(34): 3669–3750, 2002. doi: [https://doi.org/10.1016/S0045-7825\(02\)00286-4](https://doi.org/10.1016/S0045-7825(02)00286-4).
- J. A. Evans and T. J. R. Hughes. Isogeometric divergence-conforming B-splines for the steady Navier–Stokes equations. *Mathematical Models and Methods in Applied Sciences*, 23: 1421–1478, 2013.
- E. H. Georgoulis, E. Hall, and J. M. Melenk. On the suboptimality of the p -version interior penalty discontinuous Galerkin method. *Journal of Scientific Computing*, 42(1):54, 2009. doi: 10.1007/s10915-009-9315-z. URL <https://doi.org/10.1007/s10915-009-9315-z>.
- T. V. Gerya, D. Bercovici, and T. W. Becker. Dynamic slab segmentation due to brittle-ductile damage in the outer rise. *Nature*, 599:245–250, 2021. doi: <https://www.nature.com/articles/s41586-021-03937-x>.

- V. Girault and P. Raviart. *Finite Element Methods for Navier-Stokes Equations Theory and Algorithms*. Springer-Verlag, 1986.
- A. J. P. Gülcher, M. D. Ballmer, and P. J. Tackley. Coupled dynamics and evolution of primordial and recycled heterogeneity in Earth’s lower mantle. *Solid Earth*, 12:2087–2107, 2021. doi: 10.519/se-12-2087-2021.
- J. W. Hernlund and P. J. Tackley. Modeling mantle convection in the spherical annulus. *Physics of the Earth and Planetary Interiors*, 171(1):48–54, 2008. ISSN 0031-9201. doi: <https://doi.org/10.1016/j.pepi.2008.07.037>.
- P. Houston and N. Sime. Automatic symbolic computation for discontinuous Galerkin finite element methods. *SIAM Journal on Scientific Computing*, 40:C327–C357, 2018. doi: 10.1137/17M1129751.
- G. T. Jarvis and D. P. McKenzie. Convection in a compressible fluid with infinite Prandtl number. *Journal of Fluid Mechanics*, 96:515–583, 1980.
- P. Jenny, S. Pope, M. Muradoglu, and D. Caughey. A hybrid algorithm for the joint PDF equation of turbulent reactive flows. *Journal of Computational Physics*, 166(2):218–252, 2001. ISSN 00219991. doi: 10.1006/jcph.2000.6646.
- V. John, A. Linke, C. Merdon, M. Neilan, and L. G. Rebholz. On the divergence constraint in mixed finite element methods for incompressible flows. *SIAM Review*, 59(3):492–544, 2017. doi: 10.1137/15M1047696.
- T. D. Jones, N. Sime, and P. E. van Keken. Burying Earth’s primitive mantle in the slab graveyard. *Geochemistry, Geophysics, Geosystems*, 22:e2020GC009396, 2021. doi: 10.1029/2020GC009396.
- R. C. Kirby and A. Logg. A compiler for variational forms. *ACM Transactions on Mathematical Software*, 32(3), 2006.
- U. Kopitzke. Finite element convection models: comparison of shallow and deep mantle convection, and temperatures in the mantle. *Journal of Geophysics*, 46(1):97–121, 1979.
- M. Li and A. K. McNamara. Evolving morphology of crustal accumulations in Earth’s lowermost mantle. *Earth and Planetary Science Letters*, 577, 2022. doi: 10.1016/j.epsl.2021.117265. Art No 117265.
- A. Logg, K.-A. Mardal, and G. N. Wells, editors. *Automated Solution of Differential Equations by the Finite Element Method*, volume 84 of *Lecture Notes in Computational Science and Engineering*. Springer, 2012.
- J. M. Maljaars, R. J. Labeur, N. Trask, and D. Sulsky. Conservative, high-order particle–mesh scheme with applications to advection-dominated flows. *Computer Methods in Applied Mechanics and Engineering*, 348:443–465, 2019. ISSN 0045-7825. doi: 10.1016/j.cma.2019.01.028.
- J. M. Maljaars, C. N. Richardson, and N. Sime. LEOPart: a particle library for FEniCS. *Computers & Mathematics with Applications*, 81:289–315, 2021. doi: 10.1016/j.camwa.2020.04.023.

- R. McDermott and S. Pope. The parabolic edge reconstruction method (PERM) for Lagrangian particle advection. *Journal of Computational Physics*, 227(11):5447–5491, 2008. ISSN 00219991. doi: 10.1016/j.jcp.2008.01.045.
- L. S. D. Morley. The triangular equilibrium element in the solution of plate bending problems. *The Aeronautical Quarterly*, 19(2):149–169, 1968.
- A. E. Pusok, B. J. P. Kaus, and A. Popov. On the quality of velocity interpolation schemes for marker-in-cell method and staggered grids. *Pure and Applied Geophysics*, 174:1071–1089, 2017. doi: 10.1007/s00024-016-1431-8.
- P.-A. Raviart and J. M. Thomas. A mixed finite element method for 2nd order elliptic problems. In I. Galligani and E. Magenes, editors, *Mathematical Aspects of Finite Element Methods*, volume 606, pages 292–315, Berlin, Heidelberg, 1977. Springer Berlin Heidelberg.
- S. Rhebergen and G. N. Wells. A hybridizable discontinuous Galerkin method for the Navier–Stokes equations with pointwise divergence-free velocity field. *Journal of Scientific Computing*, 76:1484–1501, 2018.
- S. Rhebergen and G. N. Wells. An embedded–hybridized discontinuous Galerkin finite element method for the Stokes equations. *Computer Methods in Applied Mechanics and Engineering*, 358:112619, 2020. ISSN 0045-7825. doi: 10.1016/j.cma.2019.112619.
- Y. Ricard. Physics of mantle convection. In G. Schubert, editor, *Treatise on Geophysics (2nd edition), Volume 7 "Mantle Dynamics" (Bercovici, D (ed.)) pp 23–71*. Elsevier, Amsterdam, The Netherlands, 2015. doi: 10.1016/B978-0-444-53802-4.00132-9.
- H. Samuel. A deformable particle-in-cell method for advective transport in geodynamic modelling. *Geophysical Journal International*, 214(3):1744–1773, 06 2018. ISSN 0956-540X. doi: 10.1093/gji/ggy231.
- G. Schubert, D. L. Turcotte, and P. Olson. *Mantle Convection in the Earth and Planets*. Cambridge University Press, Cambridge, United Kingdom, 2001.
- L. R. Scott and M. Vogelius. Norm estimates for a maximal right inverse of the divergence operator in spaces of piecewise polynomials. *ESAIM: Mathematical Modelling and Numerical Analysis*, 19:111–143, 1985.
- M. W. Scroggs, J. S. Dokken, C. N. Richardson, and G. N. Wells. Construction of arbitrary order finite element degree-of-freedom maps on polygonal and polyhedral cell meshes. *ACM Transactions on Mathematical Software*, 48(2), 2022. ISSN 0098-3500. doi: 10.1145/3524456.
- N. Sime. C^0 -robust interior penalty Galerkin streamfunction formulation supporting code. <https://github.com/nate-sime/C0-RIPG-streamfunction>, 2023.
- N. Sime, J. M. Maljaars, C. R. Wilson, and P. E. van Keken. An exactly mass conserving and pointwise divergence free velocity method: application to compositional buoyancy driven flow problems in geodynamics. *Geochemistry, Geophysics, Geosystems*, 22:e2020GC009349, 2021. doi: 10.1029/2020GC009349.
- N. Sime, C. R. Wilson, and P. E. van Keken. A pointwise conservative method for thermochemical convection under the compressible anelastic liquid approximation. *Geochemistry, Geophysics, Geosystems*, 23(2):e2021GC009922, 2022. doi: <https://doi.org/10.1029/2021GC009922>.

- M. Suri. The p -version of the finite element method for elliptic equations of order $2l$. *ESAIM: Mathematical Modelling and Numerical Analysis*, 24(2):265–304, 1990.
- P. J. Tackley. Modelling compressible mantle convection with large viscosity contrasts in a three-dimensional spherical shell using the yin-yang grid. *Physics of the Earth and Planetary Interiors*, 171:7–18, 2008. doi: 10.1016/j.pepi.2008.080.005.
- P. J. Tackley and S. D. King. Testing the tracer ratio method for modeling active compositional fields in mantle convection simulations. *Geochemistry, Geophysics, Geosystems*, 4:8302, 2003. doi: 10.1029/2001GC000214.
- N. Tosi, C. Stein, L. Noack, C. Hüttig, P. Maierová, H. Samuel, D. R. Davies, C. R. Wilson, S. C. Kramer, C. Thieulot, A. Glerum, M. Fraters, W. Spakman, A. Rozel, and P. J. Tackley. A community benchmark for viscoplastic thermal convection in a 2-D square box. *Geochemistry, Geophysics, Geosystems*, 16(7):2175–2196, 2015. doi: 10.1002/2015GC005807.
- P. E. van Keken, C. J. Spiers, A. P. van den Berg, and E. J. Muzyert. The effective viscosity of rocksalt: implementation of steady-state creep laws in numerical models of salt diapirism. *Tectonophysics*, 225:457–476, 1993. doi: 10.1016/0040-1951(93)90310-G.
- P. E. van Keken, S. D. King, H. Schmeling, U. R. Christensen, D. Neumeister, and M.-P. Doin. A comparison of methods for the modeling of thermochemical convection. *Journal of Geophysical Research*, 102:22477–22495, 1997. doi: 10.1029/97JB01353.
- I. Wada and S. D. King. Dynamics of subducting slabs: Numerical modeling and constraints from seismology, geoid, topography, geochemistry, and petrology. In G. Schubert, editor, *Treatise on Geophysics (2nd edition), Volume 7 "Mantle Dynamics" (Bercovici, D (ed.)) pp 339–391*. Elsevier, Amsterdam, The Netherlands, 2015. doi: 10.1016/B978-0-444-53802-4.00132-9.
- H. Wang, R. Agrusta, and J. van Hunen. Advantages of a conservative velocity interpolation (CVI) scheme for particle-in-cell methods with application in geodynamic modeling. *Geochemistry, Geophysics, Geosystems*, 16(6):2015–2023, 2015. doi: 10.1002/2015GC005824.
- T. Warburton and J. S. Hesthaven. On the constants in hp -finite element trace inverse inequalities. *Computer Methods in Applied Mechanics and Engineering*, 192(25):2765–2773, 2003. ISSN 0045-7825. doi: [https://doi.org/10.1016/S0045-7825\(03\)00294-9](https://doi.org/10.1016/S0045-7825(03)00294-9).